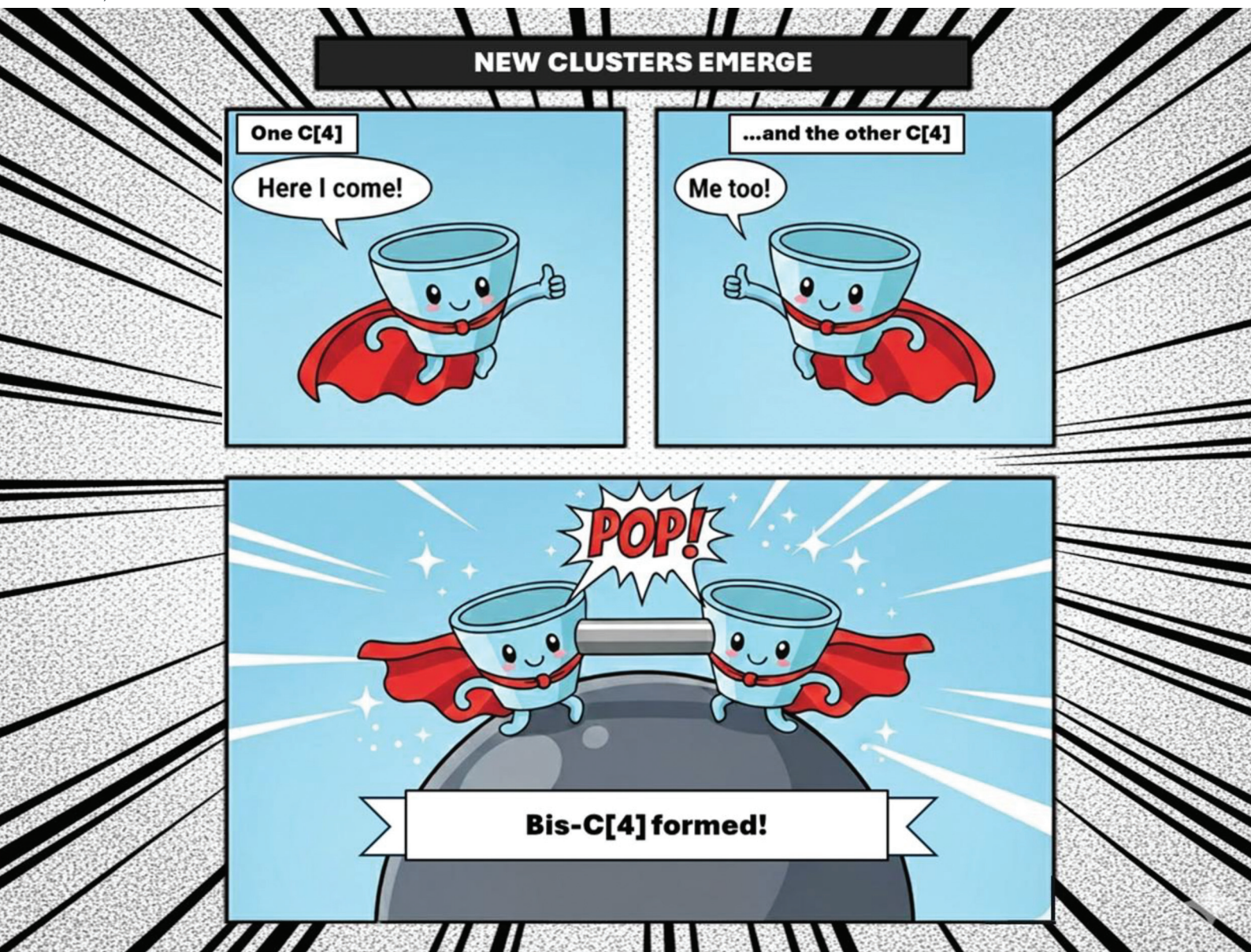


Dalton Transactions

An international journal of inorganic chemistry



rsc.li/dalton



ISSN 1477-9226

Cite this: *Dalton Trans.*, 2025, **54**,
16643

The coordination chemistry of 2,2'-bis-*p*-^tBu-calix[4]arene

Scott J. Dalgarno *^a and Euan K. Brechin *^b

A review of the coordination chemistry of 2,2'-bis-*p*-^tBu-calix[4]arene (H₈bisTBC[4]) reveals thirteen published structures, seven of which are homometallic complexes of manganese (x5) and copper (x2), and six which are heterometallic 3d–4f (4 × Mn–Gd, 1 × Fe–Gd and 1 × Cu–Tb). In the majority of cases the disposition of the inverted, fully deprotonated bisTBC[4] ligand favours the formation of [M₄] butterflies, with two metals housed in the polyphenolic TBC[4] pockets and two encapsulated in the space between the pockets. The dominant structure directing ability of the ligand is reflected in the similarity of compounds made, despite the differences in the metal ions employed. Indeed, in some 3d–4f cases transition metals (TM) and lanthanide metals (LnM) can be swapped out whilst retaining isostructural topologies. The metal ion binding rules established for TBC[4] are carried forward for bisTBC[4] such that chelating to TM^{III} is favoured over TM^{II} which is favoured over LnM^{III}. The addition of co-ligands is found to be both complementary and counter-complementary to cluster growth. Magnetic susceptibility and magnetisation data reveal the presence of both ferro- and antiferromagnetic exchange interactions in the mixed valent Mn species and the 3d–4f clusters. Strong antiferromagnetic exchange dominates the magnetism of the Cu^{II} compounds. Magneto-structural correlations aligned to theory are discussed for some of the Mn-based compounds.

Received 19th September 2025,
Accepted 18th October 2025

DOI: 10.1039/d5dt02246k

rsc.li/dalton

Introduction

Calixarenes are cyclic polyphenols that are well-known for their ability to play host to a vast range of guest molecules depending on their chemical makeup. Many of these hosts are

derived from the parent *p*-^tBu-calix[*n*]arene analogues shown schematically in Fig. 1A, hereafter termed H_{*n*}TBC[*n*]s (where *n* represents the number of aromatic rings present in the framework and H_{*n*} indicates the degree of protonation/deprotonation at the lower-rim). H_{*n*}TBC[*n*]s are readily de-*tert*-butylated and functionalised at the upper-rim, modified at the lower-rim, e.g. via Williamson ether formation, or adapted at the methylene bridges with substituents at either equatorial or axial positions.¹ From coordination chemistry and magnetism perspectives, the parent H_{*n*}TBC[*n*]s are extremely attractive

^aInstitute of Chemical Sciences, Heriot-Watt University Riccarton, Edinburgh, Scotland EH14 4AS, UK. E-mail: S.J.Dalgarno@hw.ac.uk^bEaStCHEM School of Chemistry, The University of Edinburgh, David Brewster Road, Edinburgh, EH9 3FJ Scotland, UK ebrechin@ed.ac.uk

Scott J. Dalgarno

Scott J. Dalgarno is Chair of Supramolecular Chemistry at Heriot-Watt University. His research interests are in self-/metal-directed assembly, crystal engineering, host-guest chemistry and energetic materials. He has been the recipient of the Royal Society of Chemistry Harrison-Meldola Memorial and Sir Edward Frankland prizes, and the Chemical Communications Emerging Investigator Lectureship.



Euan K. Brechin

Euan K. Brechin is the Crum Brown Chair of Chemistry at The University of Edinburgh. His research interests are in synthetic coordination chemistry and molecular magnetism. He has been the recipient of the Royal Society of Chemistry Mond-Nyholm, Tilden, Corday-Morgan, Chemistry of the Transition Metals and Sir Edward Frankland prizes.



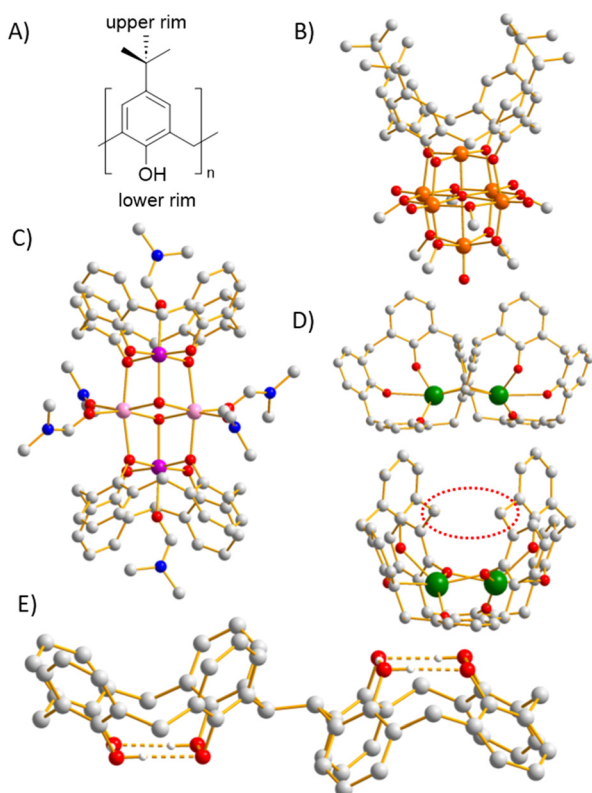


Fig. 1 (A) Schematic for $H_nTBC[n]$ s indicating the different regions of the general molecular framework. (B) TBC[4]-supported polyoxovanadate showing bridging of TBC[4] between neighbouring V centres. (C) Partial structure of a TBC[4]-supported $[Mn^{III}Mn^{II}(\mu_3-OH)_2]$ butterfly. (D) Two views of a partial structure of a TBC[8]-supported LnM^{III} dimer showing the clash between methylene groups at the centre of the complex as indicated by the dashed red ellipse. (E) Partial structure of $H_8bisTBC[4]$ showing H-bonding interactions occurring at the constituent $H_4TBC[4]$ lower-rims. Colour code: C = grey, H = white, N = blue, O = red, V = orange, Mn^{III} = magenta, Mn^{II} = pink, LnM = green. Figures are not to scale. Some t Bu groups and ligated solvent/solvent of crystallisation have been omitted for clarity. H atoms are omitted in B–D.

ligands for the formation of polynuclear clusters of 3d or 4f ions, as well as 3d–4f ion mixtures. This is attributable to the lower-rim phenolic groups that can be deprotonated with ease and that are also capable of bridging to neighbouring metal ions within a prevailing assembly. Conformational versatility in the general calixarene framework increases concomitantly with ring size and, with the content of this review in mind, it is noteworthy that calix[4]arenes adopt four main conformations (or slight variations of these between the extremes), these being cone, partial cone, 1,2- and 1,3-alternate.²

Our work in TBC[n]-supported cluster formation began with $H_4TBC[4]$ in 2009, and at that point there was only one TBC[4]-supported polynuclear cluster in the literature that had not been synthesised under air-sensitive conditions, this being a polyoxovanadate ($[V_6]$) reported by Luneau and co-workers (Fig. 1B).³ This species was formed under solvothermal conditions, and inspection of the structure shows that a TBC[4] cone caps a vertex of the cluster with lower-rim O atoms μ -brid-

ging. It is worth noting that numerous other TBC[4]-supported, predominantly Ti-based polynuclear clusters had also been reported at that time using air-sensitive conditions,⁴ but these will not be discussed further as this contribution is concerned solely with systems isolated *via* protocols in which oxygen is present. Our first success in this area came from the reaction of $H_4TBC[4]$ with Mn^{II} halides in a dmf/MeOH solvent mixture and in the presence of Et_3N as a base.⁵ The reaction does not proceed until addition of base, but within 1 hour produces a dark microcrystalline precipitate. Filtration and standing of the solution delivers diffraction quality single crystals in hours/overnight, analysis of which shows these to be a TBC[4]-supported cluster of formula $[Mn^{III}Mn^{II}(OH)_2(TBC[4])_2(dmf)_6]$ (Fig. 1C) in which Mn^{III} and Mn^{II} ions occupy wing and body positions of a $[Mn^{III}Mn^{II}(\mu_3-OH)_2]$ butterfly, respectively. Interestingly, the binding pocket of TBC[4] in a cone conformation is pre-disposed to bind a Jahn–Teller distorted Mn^{III} ion, with four short equatorial bonds and two longer axial bonds, perfectly. In turn this drives an oxidation state distribution that is the opposite to that typically observed for $[Mn^{III}Mn^{II}(\mu_3-O)_2]$ butterflies.⁶ PXRD analysis of the precipitate and comparison with a pattern generated from SCXRD studies reveals these to be the same material, and when crops are combined, this cluster forms in near-quantitative yield. The TBC[4]-supported $[Mn^{III}Mn^{II}]$ butterfly topology is now known to form under a range of different solvent mixtures and/or Mn^{II} salts,⁷ and is a benchmark reaction for cluster formation with any new calix[4]arene-based ligand developed in the course of our work in this area.

By subsequently screening a series of reactions between $H_4TBC[4]$ and transition metal salts under ambient conditions we were able to establish empirical metal ion binding rules that have been found to be remarkably consistent as our research efforts have progressed; TBC[4] preferentially binds TM^{III} ions, will bind TM^{II} in the absence of TM^{III} ions, and will bind LnM^{III} ions in the absence of both. One naturally assumes that transitioning from TBC[4] to TBC[8] would be a simple progression from binding one to two 3d ions. This is not the case, and the tendency for TBC[8] to adopt a double-cone/taco conformation upon complexation (Fig. 1D), coupled with the methylene groups pointing towards each other at the pinch point, means that the metal ion binding pockets at the lower-rim are slightly larger and are thus far better suited to 4f ions.⁸ Indeed, it is possible to form a series of TBC[8]-supported Ln_2 clusters,^{8a} or larger polynuclear clusters in which this structural fragment is present in a double vertex capping capacity.^{8b} It should be noted that it is possible to form *e.g.* polynuclear TBC[8]-supported Mn clusters,⁹ but to our knowledge this can only be achieved under solvothermal conditions.

With a desire to extend the binding rules and capping behaviour established for TBC[4] in a systematic manner, the emergence of 2,2'-bis-*p*-*t*Bu-calix[4]arene ($H_8bisTBC[4]$) in the literature was a welcome development. As reported by Fantini and co-workers,¹⁰ methylation of the lower-rim of $H_4TBC[4]$ followed by lithiation using n BuLi leads exclusively to monolithiation of a methylene bridge. Subsequent reaction with



bonds and one or two longer axial bonds. The structurally more flexible Mn^{II} ions then fill the central body positions between the constituent TBC[4] lower rims, creating the inverted [Mn^{III}(wing)Mn^{II}(body)] butterfly. Comparing the coordination chemistry in **1** with that of [Mn^{III}Mn^{II}(OH)₂(TBC[4])₂(dmf)₆], one can clearly see that directly tethering two TBC[4] sub-units through a methylene bridge very effectively translates structural features/preferences of TBC[4] to bisTBC[4].

In the extended structure neighbouring clusters pack in a head-to-tail fashion *via* long contacts between the terminally bonded dmf molecules on one cluster and the (disordered)[†] Cl⁻/HCOO⁻ atoms on the second cluster, forming [Mn₈]₂ pairs. Each pair is then oriented perpendicular to adjacent [Mn₈]₂ units, with the closest contacts being between neighbouring ^tBu groups. The result is that molecules assemble into infinite chains in the *ab* plane. Perpendicular to this lie four molecules of **1** that assemble around a central solvent-filled channel, extending to the formation of aesthetically pleasing tube-like structures.¹³

Magnetic susceptibility and magnetisation data collected for **1** reveal the presence of both ferro- and antiferromagnetic exchange interactions. A simultaneous fit of the data afforded best-fit parameters of $J_{\text{Mn(III)-Mn(II)}} = +0.92 \text{ cm}^{-1}$, $J_{\text{Mn(II)-Mn(II)}} = -4.48 \text{ cm}^{-1}$ and $J_{\text{Mn(III)-Mn(III)}} = -1.52 \text{ cm}^{-1}$ ($\hat{H} = -2 \sum_{i < j} J_{ij} \hat{s}_i \cdot \hat{s}_j$).¹³ These values are in good agreement with

the parameters previously determined for molecules containing the same inverted butterfly topology of Mn^{III} and Mn^{II} centres, including the archetypal cluster [Mn^{III}Mn^{II}(OH)₂(TBC[4])₂(dmf)₆].⁵ We note that Mn^{III}-Mn^{II} exchange interactions are often found to be weakly ferromagnetic,¹⁴ and that Mn^{II}-Mn^{II} exchange interactions are invariably weakly antiferromagnetic.¹⁵ The above parameters result in a ground state of *S* = 0 with numerous excited spin-states lying in very close proximity.

Compound **1** is made using a 2 : 1 ratio of metal salt : calixarene and a detailed examination of the effect of these ratios and crystallisation conditions affords two new complexes, **2** and **3**. Repeating the reaction that produced **1** but with a metal salt : calixarene ratio of 8 : 1 and crystallising *via* slow evaporation of the dmf/MeOH mother liquor results in the formation of [Mn^{III}₆Mn^{II}₄(bisTBC[4])₂(μ₃-O)₂(μ₃-OH)₂(μ-MeO)₄(H₂O)₄(dmf)₈·4dmf (2·4dmf).¹⁶ The crystal structure of 2·4dmf was solved in the triclinic space group *P* $\bar{1}$ (Fig. 3), with the asymmetric unit comprising half of the formula. Initial inspection of the structure shows that it is closely related to **1**, again comprising of two offset, asymmetric [Mn^{III}₂Mn^{II}₂(μ₃-OH)(μ-OR)₄] butterflies, with the Mn^{III} (Mn1, Mn2 and symmetry equivalent, *s.e.*) and Mn^{II} (Mn3, Mn4) ions occupying the wing and body butterfly positions, respectively. The μ₃-OH⁻ ion (O6) bridges between Mn4-Mn5 and to the peripheral Mn1. The four edges of the butterfly are μ-bridged by an O atom of the same calixarene ligand. In this case, however, there is an additional [Mn^{III}₂(μ₃-O)₂] dimer (Mn3, O3 and *s.e.*) that sits in the centre of the cluster, linking the two

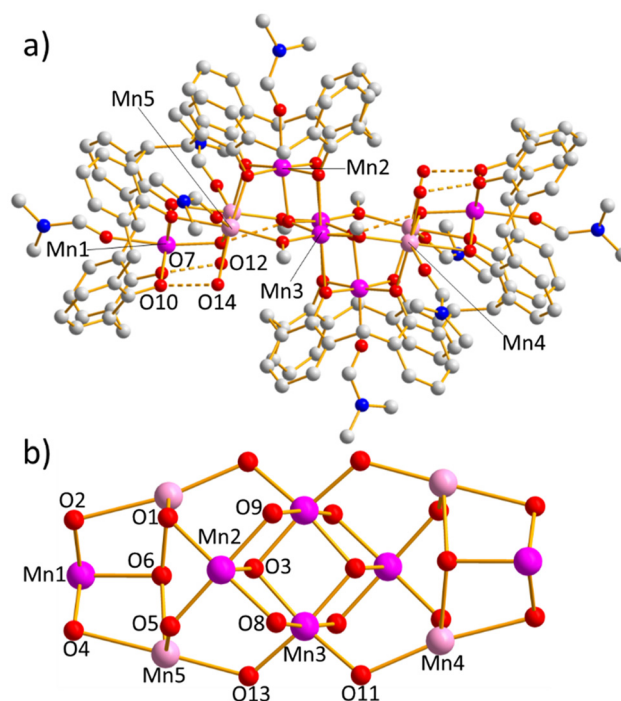


Fig. 3 (a) Molecular structure of complex **2**. (b) Metal–oxygen core of **2**. Colour code: Mn^{III} = magenta, Mn^{II} = pink, O = red, N = blue, C = grey. H atoms, ^tBu groups and solvent of crystallisation removed for clarity.

butterflies together. Thus, O3 and O3' bridge between Mn3 and Mn3' in the dimer and to Mn2 and Mn2' in the butterflies, O3 also being H-bonded to the μ₃-OH⁻ ion (O6, O6') in the [Mn₄] butterfly (O...^(H)O, ~2.7 Å). The [Mn^{III}₂(μ₃-O)₂] dimer is further connected to the Mn^{II} ions in the butterflies by a total of four μ-MeO⁻ ions (O11, O13 and *s.e.*).

The calixarenes are fully deprotonated and adopt the same conformation as in **1** and bond in a similar manner, though are μ₆-bridging. Two O atoms (O7, O10) are terminally bonded at the periphery of the cluster to Mn1, four are μ-bridging within each [Mn₄] butterfly (O1, O2, O4, O5), and two are μ-bridging between the [Mn₄] butterfly and the [Mn^{III}₂(μ₃-O)₂]²⁺ dimer (O8, O9), *i.e.*, between Mn2/Mn2'-Mn3/Mn3'. The Mn^{III} ions all sit in the TBC[4] pockets, each further bonded to a dmf molecule that fills the ligand cavity. The Mn^{III} ions are thus six coordinate ($\{\text{MnO}_6\}$) and in distorted octahedral geometries, with the O(dmf)...Mn-(μ₃-OH) vector defining the Jahn–Teller axis. The Mn^{II} ions are also six coordinate and in distorted ($\{\text{MnO}_6\}$) octahedral geometries, their coordination spheres being completed by one dmf and one H₂O molecule (O12, O14) per metal. The latter are H-bonded to the terminally bonded phenolate O atoms (O...^(H)O, ~2.6 Å). Note that the four central Mn^{III} ions (Mn2, Mn5 and *s.e.*) also form a [Mn^{III}₄O₂]⁸⁺ butterfly, and thus an alternative description of the metallic skeleton of **2** is of three vertex- and edge-sharing butterflies, the central butterfly being perpendicular to the other two.



The four dmf molecules of crystallisation are associated with the upper rims of the TBC[4] moieties, with close contacts to the bonded dmf molecule in the cavity ($O\cdots(H)C$, ~ 2.6 Å) and longer contacts to the ^tBu groups ($O\cdots(H)C$, ~ 3.3 – 3.6 Å). The closest inter-cluster contacts are between the dmf molecules bonded to the Mn^{II} ions and the C(H) atoms of the calixarenes (>3.4 Å). In the extended structure molecules of **2** are packed in sheets, separated by the dmf molecules of crystallisation.

Magnetic susceptibility and magnetisation data for **2** reveal the co-existence of (weak) ferro- and antiferromagnetic exchange interactions, as seen for **1**. The size and structural complexity of **2** precludes a quantitative fit of the experimental data, but the interactions were studied in detail theoretically *via* DFT calculations, alongside complex **3** (see below).

If the reaction that produced **1** is repeated, but with a metal:calixarene ratio of 6:1 the complex $[\text{Mn}_4^{\text{III}}\text{Mn}_6^{\text{II}}(\text{bisTBC}[4])_2(\mu_3\text{-OH})_4(\mu\text{-OH})_4(\text{MeOH})_4(\text{dmf})_4(\text{MeCN})_2]\cdot\text{MeCN}$ (**3**·MeCN) is formed.¹⁷ The crystal structure of **3**·MeCN was solved in the monoclinic, space group $P2_1/n$ with half of the formula in the asymmetric unit (Fig. 4). A comparison of the formulae and structures of **2** and **3** reveal them to be very similar, but with several intriguing differences. (a) The oxidation states of the two metal ions (Mn5 and s.e.) in the central $[\text{Mn}_2\text{O}_2]$ dimer of **3** are different, being Mn^{II} rather than Mn^{III} , with concomitant increases in the bond lengths around these metal ions. (b) The μ_3 -bridging O atoms (O9 and

s.e.) in the central $[\text{Mn}_2\text{O}_2]$ dimer of **3** connecting Mn5/Mn5' to each other and to Mn4/Mn4' are $\mu_3\text{-OH}^-$ in **3** but $\mu_3\text{-O}^{2-}$ in **2**. (c) The μ -bridging groups connecting the Mn5, Mn5' ions in the dimer to the Mn^{II} ions in the butterflies (Mn2, Mn3 and s.e.) are $\mu\text{-OH}^-$ in **3** but $\mu\text{-OMe}^-$ in **2**. (d) MeCN molecules sit in the TBC[4] cavities completing the coordination of the Mn^{III} ions in **3**, rather than the dmf molecules in **2**. (e) MeOH molecules complete the coordination of the Mn^{II} ions in **3** compared to the H_2O molecules present in **2**. The near isostructural/isomeric nature of **2** and **3** reflect the dominant structure directing effects of the bisTBC[4] ligand, with subtle changes in reaction conditions allowing isolation of molecules with different oxidation state distributions, a key feature when attempting to understand magneto-structural correlations.

Examination of the extended structure in **3** reveals that the closest intermolecular interactions are between coordinated dmf molecules and the ^tBu moieties at $C\cdots C$ distances ≥ 3.2 Å, and between neighbouring ^tBu groups at $C\cdots C$ distances ≥ 3.8 Å. The closest M \cdots M distance is ~ 12.3 Å between the Mn1 ions of distinct molecules, meaning they are structurally isolated thanks to the framework of the bisTBC[4] ligands and overall shape of the assembly.

Estimation of the magnetic exchange interactions present in both **2** and **3** were performed using DFT calculations (Fig. 5).¹⁷ For **3**, all six J values were found to be weakly antiferromagnetic, ranging between $-0.2 \leq J \leq -4.8$ cm^{-1} . Differences can be accounted for *via* magneto-structural correlations previously developed for O-bridged $\text{Mn}^{\text{III/II}}$ compounds in which the metal oxidation state, the Mn–O and Mn \cdots Mn distances, the Mn–O–Mn angles, and the orientation of Jahn–Teller axes of the Mn^{III} ions all play a significant role.¹⁸ For example, the J_1 exchange interaction is the most antiferromagnetic in **3** as it is between two Mn^{II} ions mediated *via* two $\mu_3\text{-OH}^-$ bridges with relatively short Mn–O/Mn–Mn distances and relatively small Mn–O–Mn angles.

The introduction of the two central Mn^{III} ions in **2** changes the picture to a significant extent, with the six J values now found to be in a much larger range ($+4.1 \leq J \leq -40.4$ cm^{-1}) and with both ferro- and antiferromagnetic exchange interactions present. The strongest antiferromagnetic exchange interaction (J_1) is between the two central Mn^{III} ions and is caused by the relatively small Mn–O–Mn angles and the short Mn–O and Mn \cdots Mn distances. Thus, J_1 has changed from -4.8 cm^{-1} in **3** to -40.4 cm^{-1} in **2**. The presence of parallel Jahn–Teller axes on these two metal ions classifies this moiety as a Type I dimer,^{18a} based on detailed studies of a large family of $[\text{Mn}_2^{\text{III}}(\text{OR})_2]$ complexes in which a large J_{AF} contribution and a negligible J_{F} contribution to the exchange would be expected. J_5 in **2**, between two Mn^{III} ions bridged by a $\mu_3\text{-O}^{2-}$ ion and a $\mu\text{-OR}^-$ group, is also weakly ferromagnetic. In this case this moiety can be classified as a Type II dimer unit in which the Jahn–Teller axes of the Mn^{III} ions lie co-parallel and along $\mu\text{-O}^{2-}$ bridge.^{18a} This leads to borderline ferro/antiferromagnetic coupling dictated by the Mn–O–Mn angles and Mn–O distances. J_2 is also ferromagnetic in nature, mediated between Mn^{II} – Mn^{III} ions *via* a

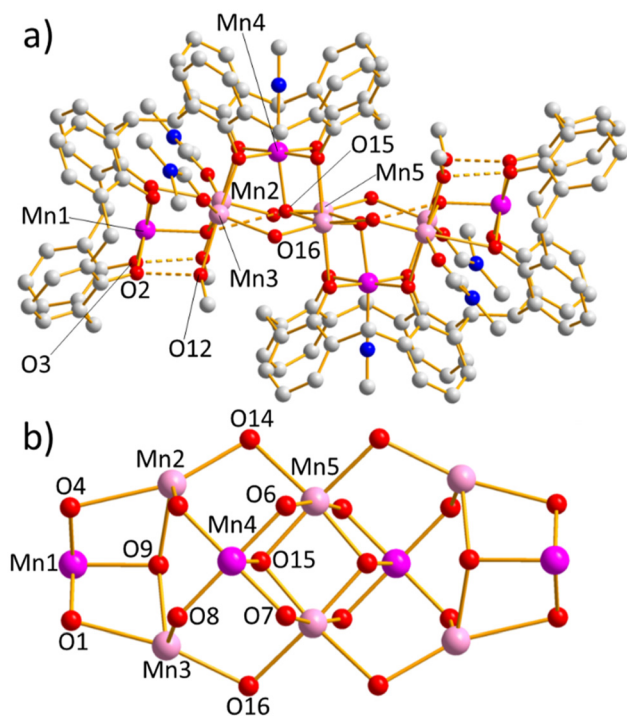


Fig. 4 (a) Molecular structure of complex **3**. (b) Metal–oxygen core of **3**. Colour code: Mn^{III} = magenta, Mn^{II} = pink, O = red, N = blue, C = grey. H atoms, ^tBu groups, some endo-cavity solvent, and solvent of crystallisation omitted for clarity.



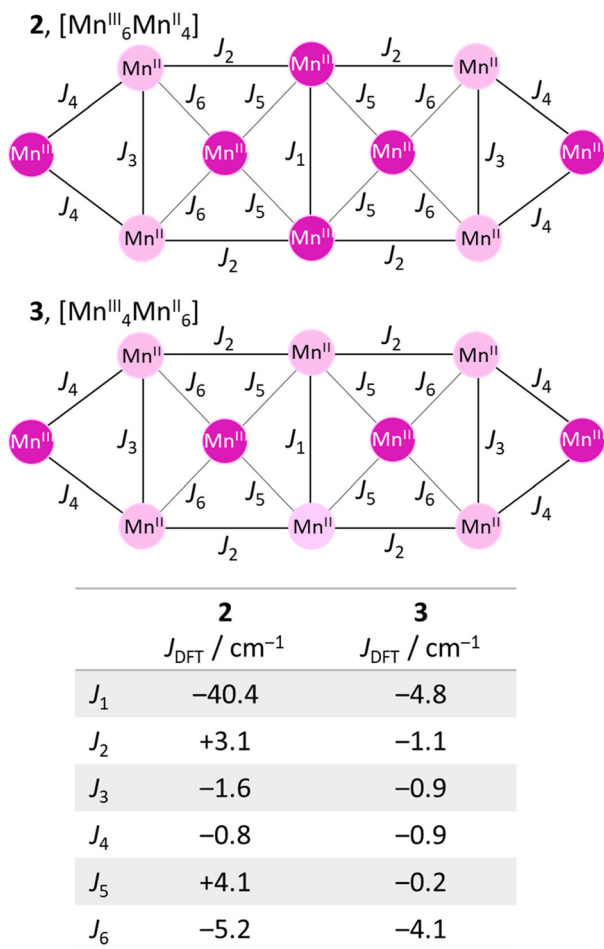
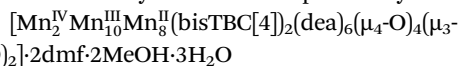


Fig. 5 Exchange interaction scheme used to calculate the J values in **2** (top) and **3** (middle) and the DFT calculated J values for both (bottom).

single $\mu\text{-OR}^-$ bridge with a short Mn–O distance and a large Mn–O–Mn angle.

In the coordination chemistry of polymetallic clusters of Mn, perhaps the most prolific/successful class of ligands are the N/O-chelates.¹⁹ This includes unsubstituted and *N*-substituted diethanolamines (R-deaH₂) and variants of 2-(hydroxymethyl)pyridine (hmpH). These flexible ligands can bridge in a number of ways, but there is often a tendency towards making [Mn₄] butterflies. Given that (a) bisTBC[4]-supported Mn clusters (**1–3**) contain similar structural units (albeit with the inverse metal oxidation state distribution), and (b) the vast majority of polymetallic clusters reported are heteroleptic not homoleptic, the combination of the two ligand types (N/O-chelate, calix[*n*]arene) may be complementary. Indeed, the remarkable influence of N/O-chelates in this reaction system is exemplified by the complex



(4·2dmf·2MeOH·3H₂O), made from the reaction of MnCl₂·4H₂O, H₈bisTBC[4] and deaH₂ (R = H) in a basic dmf/MeOH solution (Fig. 6).²⁰ The ratio of metal salt : calixarene : deaH₂ was 1 : 10 : 4, with crystals of 4·2dmf·2MeOH·3H₂O solving in the monoclinic

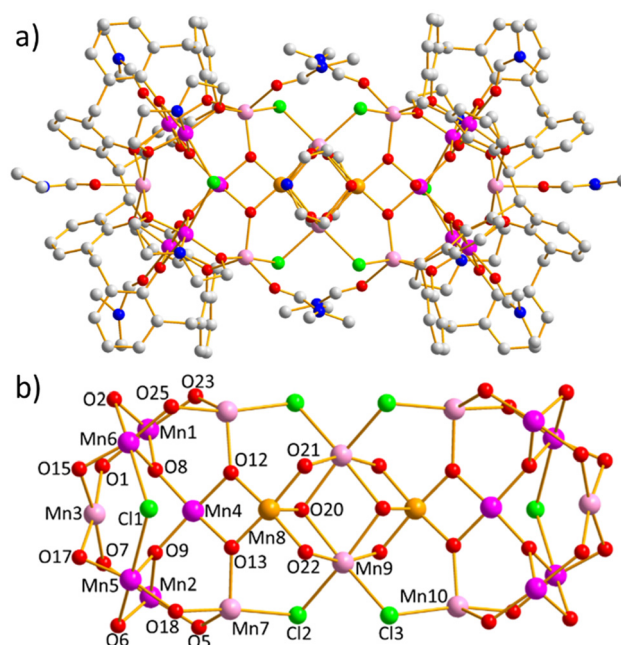


Fig. 6 (a) Molecular structure of complex **4**. (b) Metal–oxygen/halide core. Colour code: Mn^{IV} = orange, Mn^{III} = magenta, Mn^{II} = pink, O = red, N = blue, C = grey. H atoms, ^tBu groups and solvent of crystallisation are omitted for clarity.

space group C_2/c upon diffusion of Et₂O into the mother liquor. The asymmetric unit comprises half of the formula. The metallic skeleton of **4** is comprised of seven vertex-sharing [Mn₄] butterflies. The central unit is perhaps best described as a (highly unusual) [Mn₂^{IV}Mn₂^{III}(μ₃-O)₂(μ-OR)₄] butterfly, with the Mn^{IV} ions (Mn8 and s.e.) sitting on the wings and the Mn^{II} ions (Mn9, Mn9') sitting in the body positions. The two μ₃-O²⁻ ions (O20, O20') link Mn9 to Mn9' and further bridge to either Mn8 or Mn8'. The four outer edges of the butterfly that link Mn8–Mn9 (and s.e.) are each bridged by a μ-OR⁻ unit derived from two dea²⁻ ligands. These chelate to Mn8 (and Mn8'), using each O atom (O21, O22) as a μ-bridge to neighbouring Mn^{II} ions (Mn9, Mn9').

The Mn^{IV} ions are the shared vertices of the two butterflies that sit either side of, and approximately perpendicular to, the central [Mn₄] unit. These butterflies are best described as [Mn^{IV}Mn^{III}Mn₂^{II}(μ₃-O)₂] moieties. The two body positions are the shared Mn^{IV} ion (Mn8) and the Mn^{III} ion (Mn4) and the wing positions are Mn^{II} ions (Mn7, Mn10 and s.e.). The body ions are linked to each other and the wings by a μ₃-O²⁻ ion (O12, O13 and s.e.). These [Mn^{IV}Mn^{III}Mn₂^{II}(μ₃-O)₂] butterflies are further connected to the central [Mn₂^{IV}Mn₂^{II}(μ₃-O)₂(μ-OR)₄] unit by four Cl⁻ ions that bridge between the Mn^{II} ions (Mn7–Cl2–Mn9, Mn10–Cl3–Mn9). There are four further butterflies, two at each end of the cluster, linked to each other and to the [Mn^{IV}Mn^{III}Mn₂^{II}(μ₃-O)₂] units, with the Mn^{II} ions (Mn7, Mn10) being the shared vertex. These are best described as [Mn₂^{III}Mn₂^{II}(μ₄-O)(μ-OR)₅] butterflies with the Mn^{III} ions (Mn1, Mn6, Mn2, Mn5) being in the body and the Mn^{II} ions (Mn7, Mn3, Mn10)



being on the wings. Mn3 (Mn^{II}) is the shared vertex between the two peripheral butterflies. The body Mn^{III} ions are linked to each other *via* one μ -O(Ph) atom derived from a phenolate O atom of the calixarene (O2, O6), and one μ_4 -O²⁻ ion (O8), which further bridges to Mn3 in the same butterfly and to Mn4 (Mn^{III}) in the neighbouring [Mn^{IV}Mn^{III}Mn^{II}(μ_3 -O)₂] butterfly. The four outer edges of the butterfly are each bridged by a μ -OR⁻ unit derived from a bisTBC[4] ligand (O23, O25, O1, O15, O7, O17, O5, O18 and *s.e.*).

The bisTBC[4] ligands are fully deprotonated and bond in a μ_8 -fashion. All O(Ph) atoms are μ -bridging, with exception of two, O3 and O4, which are terminally bonded to Mn1 and Mn2, respectively, and H-bond to the H₂O molecule bonded to Mn4 (O...(*H*)O, \sim 2.6 Å). The only Mn ions not connected to a bis-TBC[4] ligand are the four Mn ions in the central [Mn^{IV}Mn^{II}(μ_3 -O)₂(μ -OR)₄] butterfly (Mn8, Mn9). Each Mn^{II} ion in the cluster is coordinated to one dmf molecule, and is either 5-coordinate and distorted trigonal bipyramidal, or 6-coordinate and distorted octahedral in geometry. The four Mn^{III} ions housed in the TBC[4] pockets (Mn1, Mn2) are each coordinated to a dmf molecule that sits in the ligand cavity, completing the six coordinate, distorted octahedral geometry. As with all TBC[4]-supported structures, this sits on the Jahn–Teller axis. The four Mn^{III} ions chelated by the dea²⁻ ligands (Mn5, Mn6 and *s.e.*) are also 6-coordinate and Jahn–Teller distorted with {MnO₄NCl} geometries, with the μ -Cl⁻ ion bridging between Mn5 and Mn6. The Cl⁻ ion sits on the Jahn–Teller axis of both Mn5 and Mn6. The remaining Mn^{III} ion is Mn4, which is square pyramidal, bonded to one H₂O molecule in one axial site, with a long contact to a Cl⁻ ion on the second axial site. These define the Jahn–Teller axis for Mn4.

There are numerous intramolecular H-bonding interactions and short contacts present in the structure of **4**. The O atom

(O16) of the H₂O molecule bonded to Mn4 is H-bonded to the terminally bonded O(Ph) atoms on Mn1 and Mn2 (O(*H*)...O, \sim 2.7 Å). The monodentate Cl⁻ ion on Mn5 is positioned at the centre of a triangle of N atoms derived from three dea²⁻ ligands (N...Cl, \sim 3.2–3.6 Å). The MeOH, H₂O and dmf molecules of crystallisation mediate the closest intermolecular interactions, between dea²⁻ ligands on neighbouring clusters, with numerous contacts also formed between the ligated dmf molecules/^tBu groups of the biscalixarenes. This complicated, intricate network of inter-molecular interactions leads to an aesthetically pleasing packing of the molecules in the extended structure.²⁰

Compound **4** is the largest TBC[4]-supported Mn cluster known, and the only one to contain Mn in three different oxidation states. Magnetic susceptibility and magnetisation measurements on **4** reveal the presence of weak and predominantly antiferromagnetic interactions between the constituent metal ions. The large nuclearity of the cluster, the numerous different exchange interactions, and the presence of three different metal oxidation states makes a quantitative analysis of the magnetic data impossible.

If the deaH₂ in the reaction above is swapped out for hmpH, and the anti-solvent changed to petroleum ether, crystals of [Mn^{III}₁₀Mn^{II}₄(bisTBC[4])₃(hmp)₄(μ_3 -O)₄(μ_3 -OH)₂(MeOH)₄(dmf)₆·4dmf (5·4dmf) form, and solve in the monoclinic space group *C2/c* (Fig. 7).²¹ The asymmetric unit comprises one half of the formula and symmetry expansion reveals that the centrally located bisTBC[4] ligand adopts the anti-conformation, creating two identical but ‘separate’ [Mn^{III}Mn^{II}]₂ clusters within the same molecule; the inversion centre being located at the centre of the methylene bridge link. The core of the crystallographically unique heptametallc cluster describes two perpendicular, vertex-sharing [Mn₄] but-

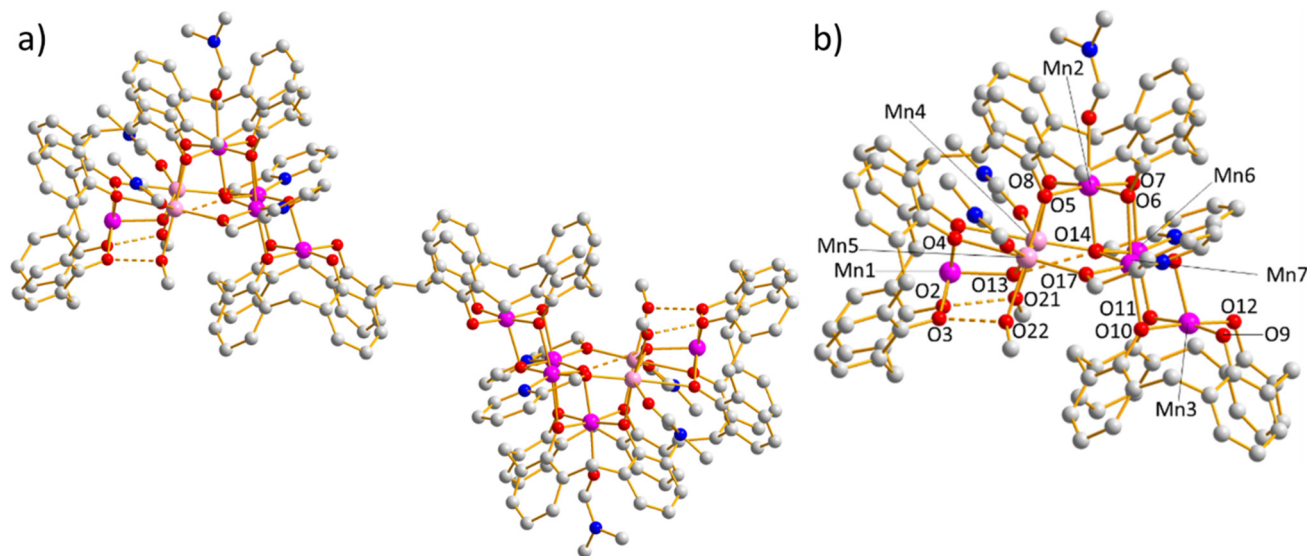


Fig. 7 (a) Molecular structure of complex **5**. (b) Selectively labelled partial ASU of complex **5** highlighting the heptametallc cluster in each half of the molecule. Colour code: Mn^{III} = magenta, Mn^{II} = pink, O = red, N = blue, C = grey. H atoms, ^tBu groups, some endo-cavity solvent, and solvent of crystallisation are omitted for clarity.



molecule, with further contacts to both the 'Bu groups of a TBC[4] moiety and a MeCN solvent of crystallisation. In the extended structure, molecules of **6** pack in offset linear chains, with closest inter-cluster Cu...Cu distances $>13 \text{ \AA}$.¹³

An alternative description of the structure of **6**, in keeping with the Mn clusters described above, is of four vertex-sharing $[\text{Cu}_4^{\text{II}}(\text{OH})(\text{OR})_4]$ butterflies that self-assemble into a wheel, encapsulating an additional Cu^{II} ion in its centre *via* the $\mu\text{-OH}^-$ ions. The structure of **6** is closely related to the tricapped trigonal prismatic $[\text{Cu}_9^{\text{II}}]$ clusters made with TBC[4],²² and ligand expansion from TBC[4] to bisTBC[4] allows for a systematic increase in cluster nuclearity. In essence, the former describes three $\{\text{Cu}^{\text{II}}\text{-TBC[4]}\}$ metalloligands encapsulating a trigonal prism, and the latter describes four $\{\text{Cu}^{\text{II}}\text{-TBC[4]}\}$ metalloligands encapsulating a square prism. Note that the core of $[\text{Cu}_9]$ is 'empty' suggesting that the inner cavity formed by the three $\{\text{Cu}^{\text{II}}\text{-TBC[4]}\}$ metalloligands is too small to accommodate an additional metal ion. The disordered metal ion at the centre of **6** perhaps suggests the space created by the four $\{\text{Cu}^{\text{II}}\text{-TBC[4]}\}$ metalloligands is actually a little too large for a single Cu^{II} ion. In turn, this suggests that it may be possible to replace/substitute the central Cu^{II} ion in **6** for larger metal ions. This would allow for a systematic study of the effect of 'guest' encapsulation upon the magnetic properties. No studies examining this have been reported, but will be a point of focus of future work with this ligand.

The magnetic properties of **6** are indicative of very strong antiferromagnetic exchange between the constituent Cu^{II} ions.¹³ A simultaneous fit of the magnetic susceptibility and magnetisation data (Fig. 9) afforded the best fit parameters, $J_1 = -84.14 \text{ cm}^{-1}$, $J_2 = -65.97 \text{ cm}^{-1}$, $J_3 = -22.69 \text{ cm}^{-1}$, where J_1 is the interaction between the vertices of the square prism through the OH^- ions, J_2 is the exchange between the Cu^{II} ions around the peripheral $[\text{Cu}_{12}]$ unit, and J_3 is the exchange between the central Cu^{II} ion and all of its nearest neighbours. With these parameters, the ground spin-state of **6** is a quadruply degenerate $S = 1/2$ state, with the first excited state being a doubly degenerate $S = 1/2$ state lying approximately 5.2 cm^{-1} higher in energy. The rest of the energy spectrum also presents a high degree of degeneracy, pointing towards significant geometric spin-frustration.

A repetition of the reaction used to make **6**, but with the addition of *N*-methyldiethanolamine (Me-deaH₂) results in the formation of $[\text{Cu}_{16}^{\text{II}}(\text{bisTBC[4]})_2(\text{Me-dea})_4(\mu_5\text{-NO}_3)_2(\mu\text{-OH})_4(\text{dmf})_{3.5}(\text{MeOH})_{0.5}(\text{H}_2\text{O})_2](\text{H}_6\text{bisTBC[4]})\cdot 16\text{dmf}\cdot 4\text{H}_2\text{O}$ ($7\cdot 16\text{dmf}\cdot 4\text{H}_2\text{O}$) when the dmf/MeOH mother liquor is allowed to slowly evaporate.²³ Crystals of $7\cdot 16\text{dmf}\cdot 4\text{H}_2\text{O}$ solve in the triclinic space group $P\bar{1}$ with the asymmetric unit comprising half the formula. The structure of **7** (Fig. 10) is very similar to that of **6**. The central metallic skeleton again defines a tetra-capped square prism, however in this case its centre is empty. The μ_8 -bridging bisTBC[4] ligands bond in same manner, chelating the face-capping Cu^{II} ions (Cu1, Cu2, and s.e.) with each O(Ph) atom μ -bridging to a Cu^{II} ion in the square prism (Cu3–Cu6). Nearest neighbour Cu^{II} ions in the upper and lower square faces of the prism are connected to each other *via* μ -

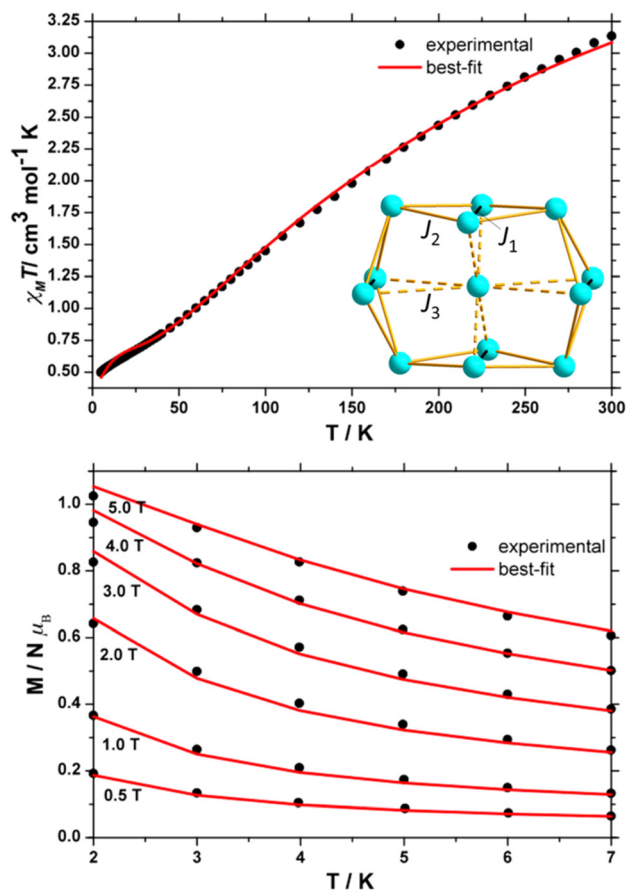


Fig. 9 Magnetic susceptibility (top) and magnetisation data (bottom) for **6**. The inset shows the exchange coupling scheme used to fit (solid red lines) the experimental data (black circles). Inset: J_1 = solid black lines, J_2 = solid gold lines, J_3 = dashed gold lines. See text for details.

OH^- ions (O9, O10), creating the same $[\text{Cu}_{13}(\text{OH})_8]$ metal-oxygen core. In this case, however, three metal ions in the same face (Cu3, Cu4, Cu6) are connected *via* a NO_3^- ion, which also H-bonds to the terminally bonded H_2O molecule on the remaining Cu^{II} in the square face (Cu5; $\text{O12}\cdots(\text{H})\text{O19}$, $\sim 2.8 \text{ \AA}$). Thus, the nitrate ions sit in and above the upper and lower square faces of the prism, preventing any further metal coordination in the cavity of the cage. The NO_3^- ions further bridge to two Cu^{II} ions (Cu7, Cu8) which cap the Cu4...Cu6 edge of the square prism. Cu7 and Cu8 are chelated by two Me-dea²⁻ ligands that bond in two different ways. The first μ_3 -bridges, using one O arm (O16) to link between Cu7–Cu8 and the other (O17) to link between Cu8 and Cu6 in the square prism. The second chelates to Cu7 with one O-arm terminally coordinated (O15) and one arm (O14) bridging to Cu4 in the square prism.

The Cu^{II} ions that sit in the tetraphenolato calixarene pockets are square planar, with a fifth, longer contact to a disordered molecule of dmf that sits in ligand cavity. The Cu^{II} ions in the square prism are five coordinate and in distorted square pyramidal geometry, the remaining sites on Cu3 and Cu5 being occupied by dmf/ H_2O molecules. The Cu^{II} ions in



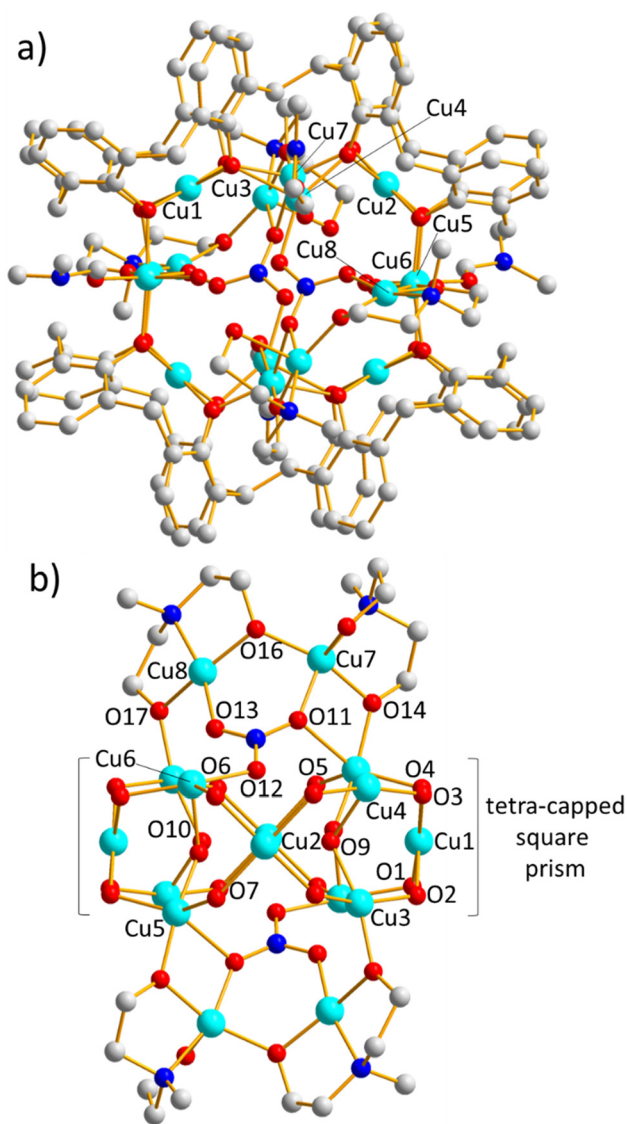


Fig. 10 (a) Molecular structure of complex 7. (b) Alternative view of the core of 7, highlighting the role of the diethanolamine and nitrate ions. Cu^{II} = pale blue, O = red, N = dark blue, C = grey. H atoms, ^tBu groups, counter ions, endo-cavity solvent, and solvent of crystallisation are omitted for clarity.

the edge-capping {Cu₂} moiety are five-coordinate, square pyramidal and four-coordinate, square planar, respectively.

The cationic [Cu₁₆]²⁺ cluster is charge balanced *via* the presence of a H₆bisTBC[4]²⁻ ion. A H₂O molecule sits in between these two units, H-bonded to one of the deprotonated O(Ph) atoms in the calixarene counter anion (O21(H)⋯O26, ~2.7 Å) and the terminally bonded O atom (O21(H)⋯O15, ~2.6 Å) of the Me-dea²⁻ ligand. This directs the formation of chains in the extended structure. Symmetry expansion shows that the [Cu₁₆] cluster is surrounded at its four 'corners' by the H₆bisTBC[4]²⁻ counter anions, resulting in them being well isolated from each other, with the closest Cu⋯Cu distances being >12 Å.²³

Magnetic susceptibility data for 7 reveal the presence of competing exchange interactions, dominated by very strong antiferromagnetic exchange. A fit of the data to a simple model using just two exchange interactions (J = the exchange between the metal ions in the {Cu₁₂} tetracapped square prism and between these metal ions and those in the {Cu₂} edge cap; J' = the exchange between the two metal ions in the edge cap), affords $J = -122 \pm 12 \text{ cm}^{-1}$ and $J' = +22 \pm 8 \text{ cm}^{-1}$. With these best-fit parameters the ground spin-state of 7 is an $S = 1$ state, with excited $S = 0, 0$ and 2 states lying 23, 35 and 46 cm^{-1} above the ground state, respectively, followed by a quasi-continuum of states. The complex topology in 7 and the numerous different exchange pathways present, aligned with the simple model used to fit the data means the obtained exchange constants should be taken with some caution. Indeed, fits with a larger number of exchange constants were not unique, the different J values being highly correlated ($-70 < J_{\text{AF}} < -100 \text{ cm}^{-1}$; $J_{\text{F}} = \sim +20 \text{ cm}^{-1}$). Note, however, that the exchange constant found in the [Cu₁₂] prism of 7 is similar to the values found in the same unit in 6 ($-66 \leq J \leq -84 \text{ cm}^{-1}$), providing some confidence those obtained for 7 are, at least, of the correct order of magnitude.

Heterometallic clusters

The first bisTBC[4]-supported heterometallic cluster reported was the complex [Mn^{III}Mn^{II}Gd^{III}(bisTBC[4])₂(Cl)₂(μ₃-OH)₄(MeOH)₂(dmf)₈·5Et₂O·5dmf (8·5Et₂O·5dmf) made from the reaction of MnCl₂·6H₂O, GdCl₃·6H₂O and H₈bisTBC[4] in a basic dmf/MeOH mixture (Fig. 11).¹³ Crystals of 8·5Et₂O·5dmf solve in the monoclinic space group $P2_1/n$ upon diffusion of Et₂O into the mother liquor. The asymmetric unit contains half the formula. The structure of 8 is remarkably similar to that of complex 1 ([Mn^{III}Mn^{II}], Fig. 2) the main difference being the replacement of two Mn^{II} ions with two Gd^{III} ions. Note that this 'metal exchange' has also been achieved for the TBC[4]-supported [Mn^{III}Mn^{II}], [Mn^{III}Mn^{II}LnM^{III}] and [Mn^{III}LnM^{III}] clusters.²⁴ The metallic skeleton of 8 describes three edge-sharing butterflies. The central butterfly is a [Mn^{II}Gd^{III}(μ₃-OH)₂(OR)₄] unit, in which the Mn^{III} ions (Mn3 and s.e.) sit in the wing positions and the Gd^{III} ions (Gd1 and s.e.) sit in the body. The μ₃-OH⁻ ions (O9) sit in the middle of this unit, bridging between the two Gd^{III} ions, further bridging to Mn3/Mn3'. The four sides of the butterfly are bridged by μ-O atoms (O7, O8) derived from the two bisTBC[4] ligands. Mn3 and Gd1 (and s.e.) are the metal ions on the shared edge of the butterflies that sit either side of the central butterfly.

This is an asymmetric [Mn^{III}Mn^{II}Gd^{III}(OH)(OR)₅] unit in which a Mn^{II} ion (Mn2) sits in a body position and a Mn^{III} ion (Mn1) sits in the peripheral wing position. There is a single μ₃-OH⁻ ion (O10) that bridges between Gd1, Mn2 and Mn1. Three of the four edges of the butterfly are occupied by single μ-bridging O(Ph) atoms from the same calixarene (O1, O4, O5), while the fourth edge is doubly bridged, *via* the shared OH⁻ ion from the central butterfly (O9) and a μ-O(Ph) atom (O8), again from the same calixarene. The latter are fully deprotonated and coordinate in a μ₅-fashion. Three O atoms are



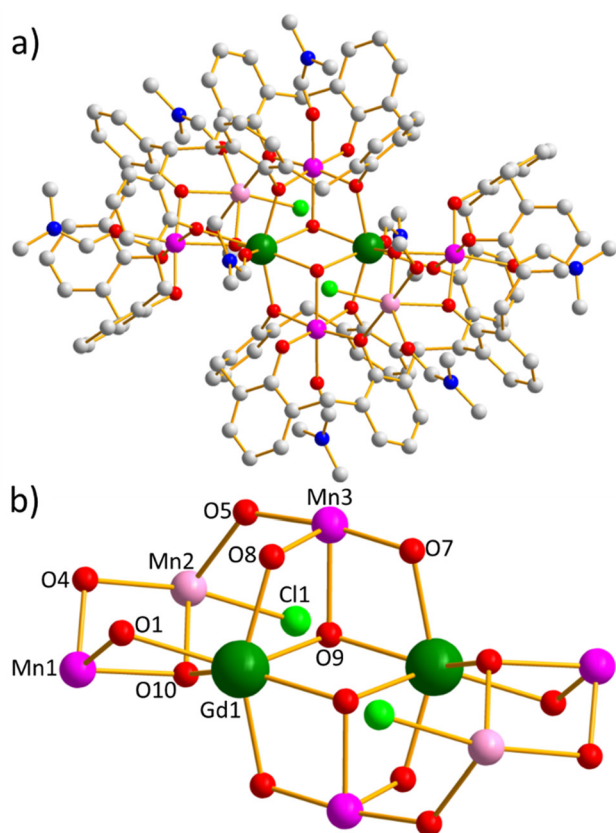


Fig. 11 (a) Molecular structure of complex **8**. (b) Metal–oxygen/halide core of **8**. Colour code: Gd^{III} = dark green, Mn^{III} = magenta, Mn^{II} = pale pink, O = red, N = blue, Cl = light green, C = grey. H atoms, ^tBu groups and solvent of crystallisation are omitted for clarity.

bonded terminally (O2, O3, O6), while the remaining five are μ -bridging; O7 and symmetry equivalent linking the two halves of the molecule together.

The remaining coordination sites on the six coordinate, distorted octahedral Mn^{II} (Mn2) sites are filled with a Cl[−] ion, a MeOH molecule and a dmf molecule. The Cl[−] ion is H-bonded to the central OH[−] ion (Cl1...^(H)O9, \sim 3.2 Å), and the O atom of the MeOH is H-bonded to one of the terminally bonded O(Ph) atoms (O15(H)...O3, \sim 2.6 Å). The Mn^{III} ions all sit in the TBC[4] pockets and are in Jahn Teller distorted octahedral geometries, coordinated to a dmf molecule that sits in the TBC[4] cavity and whose direction defines the position of the Jahn–Teller axis. There are multiple short intermolecular contacts between the Et₂O/dmf molecules of crystallisation and, primarily, ^tBu and MeOH groups on the cluster, driving the formation of a brickwork-like packing arrangement in the extended structure.¹³

The magnetic susceptibility data for **8** is indicative of the presence of both ferro- and antiferromagnetic exchange interactions being present, with the increase in the value of χT with decreasing temperature suggesting the predominance of ferromagnetic exchange and the stabilisation of a relatively large spin ground state. A fit of the susceptibility data afforded the

best fit parameters $J_{\text{Mn(III)}-\text{Mn(II)}} = +0.92 \text{ cm}^{-1}$, $J_{\text{Mn(III)}-\text{Gd(III)}} = -0.062 \text{ cm}^{-1}$, $J_{\text{Mn(II)}-\text{Gd(III)}} = +0.066 \text{ cm}^{-1}$ and $J_{\text{Gd(III)}-\text{Gd(III)}} = -0.061 \text{ cm}^{-1}$. With these parameters, the ground spin-state of **8** is an $S = 9$ state, with numerous excited spin-states lying in close proximity. As observed for **7**, the complex metal topology and the three different metal ions present means that these parameters are highly correlated, and there is no unique solution. However, their magnitude and range is entirely in keeping with that expected for Mn–Mn, Mn–Gd and Gd–Gd exchange interactions reported in the literature, to the Mn complexes discussed above, and to the related TBC[4]-supported [Mn^{III}Mn^{II}], [Mn^{III}Mn^{II}Gd^{III}] and [Mn^{III}Gd^{III}] complexes.²⁴

If the reaction used to make **8** is repeated, but the mother liquor allowed to evaporate, crystals of [Mn₄Gd₄(bisTBC[4])₂(μ_3 -OH)₄(μ -CO₃)₂(dmf)₈(H₂O)₄].MeOH·2dmf (**9**·MeOH·2dmf) are formed, and solve in the monoclinic space group $P2_1/n$ (Fig. 12),²⁵ with the asymmetric unit containing the whole formula.

The core of complex **9** contains two [Mn₂Gd^{III}(μ_3 -OH)(μ_3 -OR)₄] butterflies, linked together (and separated) by two CO₃^{2−} ions (from the fixation of atmospheric CO₂) that μ -bridge between the four Gd^{III} ions across the two butterflies (Gd1–Gd2, Gd3–Gd4). In each butterfly the Gd^{III} ions occupy the body positions and the Mn^{III} ions (Mn1, Mn2; Mn3, Mn4) occupy the wing positions. There are two μ_3 -OH[−] ions per butterfly (O1, O8; O2, O21) that bridge between the two Gd^{III} ions,

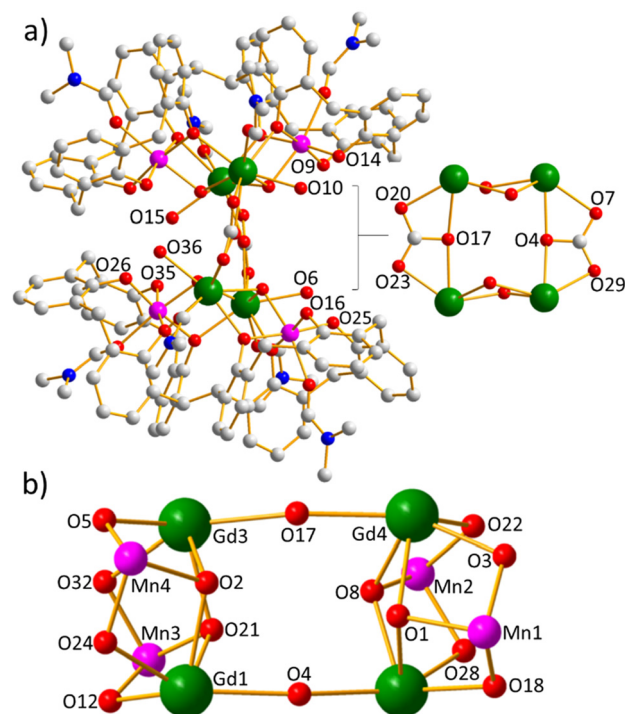


Fig. 12 (a) Molecular structure of complex **9**. (b) The metal–oxygen core of **9**. Colour code: Gd^{III} = dark green, Mn^{III} = magenta, O = red, N = blue, C = grey. H atoms, ^tBu groups and solvent of crystallisation omitted for clarity.



further linking to one of the Mn^{III} ions. Each μ_4 -bridging, fully deprotonated bisTBC[4] ligand bonds to one butterfly at the 'top' and 'bottom' of the cluster, with the four central O(Ph) atoms μ -bridging between Mn^{III}–Gd^{III} ions, and the four outer O(Ph) atoms bonding terminally to the Mn^{III} ions. The coordination spheres of the latter are completed by a dmf molecule that sits in the TBC[4] cavity in each case. It is the O atom of this molecule and the O atom of the μ_3 -OH[−] ion that defines the Jahn Teller axis of these six coordinate, octahedral metal ions. The Gd^{III} ions are chelated by a CO₃^{2−} ion, with one O atom (O4, O17) bridging between Gd^{III} ions in the two butterflies. Their coordination spheres are completed by one molecule of dmf and one molecule of H₂O. All are eight coordinate and square antiprismatic.

There are numerous intra- and intermolecular interactions, many of which are positioned between the two butterflies, that in effect help 'link' the two halves of the molecule together.²⁵ The terminally bonded O(Ph) atoms of the bisTBC[4] are H-bonded to a combination of: (a) the O atom of the H₂O molecule on a Gd^{III} ion in the same butterfly, (b) the O atom of the H₂O molecule on a Gd^{III} ion in the other butterfly, (c) the O atoms of the MeOH molecules of crystallisation, that are further H-bonded to the terminally bonded O(Ph) atoms or to the O atom of the H₂O molecule bonded to the Gd^{III} ion in the other butterfly. The effect of these (asymmetric) intramolecular H-bonds is to twist the relative positions of the two (upper and lower) butterflies such that they are not co-parallel, the [Gd₂O₂] planes being twisted by approximately 13° with respect to each other (Fig. 12a). The MeOH molecules of crystallisation are H-bonded to each other, while the dmf molecules of crystallisation have close contacts to the both the O(CO₃) atoms, and the C^t(Bu) atoms of the calixarene. The latter also have close intermolecular contacts. The result is that molecules of **9** pack in layers in the extended structure, separated by the bulky calixarene ligands.

Magnetic susceptibility and magnetisation data collected for **9** indicate the presence of competing (weak) anti- and ferromagnetic exchange interactions. In this case, the low temperature increase in χT (to 53 cm³ K mol^{−1} at 2 K) and the magnetisation saturating at $M \sim 47\mu_B$, suggests the predominance of the ferromagnetic interactions, and thus the field-induced stabilisation of a large spin ground state (the ferromagnetic ground state would be $S = 22$, $M = 44\mu_B$). The large nuclearity of the cluster, the lack of symmetry and therefore the large number of different exchange interactions precluded any quantitative fit of the magnetic data.

If the reaction used to make **9** is repeated but using Mn(NO₃)₆·6H₂O and Gd(NO₃)₃·6H₂O instead of the chloride salts, the complex [Mn₆^{III}Mn₂^{II}Gd₂^{III}(bisTBC[4])₂(μ_4 -O)₂(μ_3 -OH)₂(μ -OCH₃)₂(μ -OH)₂(MeOH)₄(dmf)₈](NO₃)₂·2H₂O (**10**·2H₂O) is formed (Fig. 13).¹³ Crystals of **10**·2H₂O solve in the monoclinic space group $P2_1/n$, with half the formula in the asymmetric unit. The structure of **10** is remarkably similar to that of **2** ([Mn₆^{III}Mn₄^{II}], Fig. 3), the only major difference being the interchange of two Mn^{II} ions for two Gd^{III} ion. Note that the Mn^{II}, Gd^{III} positions are disordered.†

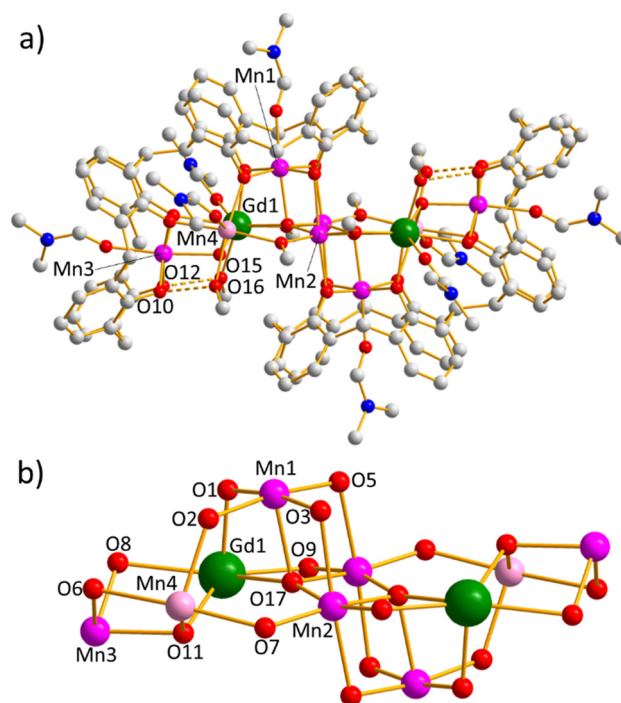


Fig. 13 (a) Molecular structure of complex **10**. (b) The metal–oxygen core of **10**. Colour code: Gd^{III} = dark green, Mn^{III} = magenta, Mn^{II} = pale pink, O = red, N = blue, Cl = light green, C = grey. H atoms, counter ions, Bu groups and solvent of crystallisation are omitted for clarity.

The metallic skeleton of **10** describes three vertex sharing butterflies. The central butterfly is [Mn₄^{III}O₂(OR)₄] and comprises four Mn^{III} ions (Mn1, Mn2 and s.e.) linked centrally by two O^{2−} ions (O17 and s.e.) that bridge between Mn2 and Mn2', further bridging to Mn1/Mn1'. The four edges of the butterfly are each μ -bridged by an O(Ph) atom (O3, O5 and s.e.) of a bisTBC[4] ligand; two originating from one calixarene and two from another. Mn1(Mn1') is the shared vertex to the peripheral butterflies which are comprised of [Mn^{III}Mn^{II}Gd^{III}O(OH)(OR)₄] units. The body positions are half occupancy Mn^{II}/Gd^{III} ions (Mn4, Gd1) with the remaining, outermost wing position being a Mn^{III} ion (Mn3, Mn3'). The O^{2−} ion (O17, O17') in the central butterfly also bridges to Gd1 (Gd1') in the peripheral butterflies. The μ_3 -OH[−] ion (O11) bridges between the body Mn^{II}–Gd^{III} ions, further linking to Mn3 (Mn^{III}). The four edges of the butterfly are μ -bridged by O(Ph) atoms (O1, O2, O6, O8) originating from the same bisTBC[4] ligand. The Mn^{III} ions in the body positions in the central butterfly (Mn2, Mn2') are linked to the Mn^{II}/Gd^{III} ions in the body positions in the peripheral butterflies by a combination of μ -OMe[−]/OH[−] ions (O7, O9). The bisTBC[4] ligands are μ_5 -bridging, with two O atoms (O10, O12) terminally bonded (to Mn3) and six μ -bridging; O5 and O3 linking the two halves of the cluster together. The Mn^{III} ions are all six coordinate and in Jahn Teller distorted octahedral geometries. The four that sit in the TBC[4] pockets are coordinated to a dmf molecule that sits in each ligand cavity, defining the elongated axis. The Jahn Teller axis



of Mn2 is the O3(Ph)–Mn2–O5(Ph) vector. Mn3 (Mn^{II}) is six coordinate and in distorted octahedral geometry, its coordination sphere completed by a molecule of dmf and a molecule of MeOH. Gd1 is heptacoordinate and in distorted pentagonal bipyramidal geometry, its coordination sphere likewise being completed by a molecule of dmf and a molecule of MeOH. The O atoms of the MeOH ligands are H-bonded to the terminally bonded O(Ph) atoms (O15(H)⋯O10, O⋯16(H), ~2.6 Å). The NO₃[−] counter anions are H-bonded to the H₂O molecules of crystallisation and have longer contacts to both the ^tBu groups of the bisTBC[4] ligands and the ligated dmf molecules.

Molecules of **10** pack in a parquet-like pattern in the extended structure with layers of clusters being perpendicular to the layers above and below. Closest inter-cluster M⋯M interactions are >14 Å. Magnetic susceptibility data for **10** are consistent with the presence of competing ferro- and antiferromagnetic exchange interactions, both being weak in magnitude. The nuclearity and structural complexity of **10** prevented a quantitative fit of the data.

Repetition of the reaction used to make **8**, but with the addition of the co-ligand 2,6-pyridinedimethanol (H₂pdm) results in the formation of [Mn^{III}Mn^{II}Gd^{III}(H₃bisTBC[4])(pdmH)(pdm)(MeOH)₂(dmf)]·3MeCN·dmf (**11**·3MeCN·dmf) upon vapour diffusion of MeCN into the basic dmf/MeOH mother liquor (Fig. 14).²⁶ Crystals of **11** solve in the tetragonal space group *P*₄₁₂₁₂ with the asymmetric unit comprising the entire formula.

The metallic skeleton of **11** describes a [Mn^{III}Mn^{II}Gd^{III}] triangle and the metal–oxygen core a [Mn^{III}Mn^{II}Gd^{III}(μ₃-OR)(μ-OR)₃]^{4−} partial butterfly. The μ₃-OR[−] atom that sits in the centre of the triangle (O3) bridging Mn1 (Mn^{III}), Mn2 (Mn^{II}) and Gd1 is derived from the pdm^{2−} ligand which chelates

Gd1. The outer edges of the triangle are all μ-bridged by O(R)[−] atoms, one (O1) from the pdmH[−] ligand that also chelates Gd1, and two (O4, O8) from the H₃bisTBC[4] ligand, the latter being μ₄-bridging. The Mn^{III} ion sits in one of the TBC[4] pockets (O4, O5, O6, O7), which is fully deprotonated, with O5 and O7 being terminally coordinated. O7 is H-bonded to the O atom of the MeOH molecule coordinated to Gd1 (O⋯(H)O, ~2.6 Å). The second H₃TBC[4] unit coordinates terminally to Mn2 *via* one O atom (O2), with O12–O14 remaining protonated and uncoordinated. O14 H-bonds to the O atom of the MeOH molecule bonded to Mn2 (O14(H)⋯(H)O15, ~2.7 Å), and all four O atoms in this calixarene unit are H-bonded to each other.

Mn1 is five coordinate and square-base pyramidal in geometry, with a sixth, longer contact to an MeCN of crystallisation that sits in the TBC[4] cavity. The cavity of the H₃TBC[4] moiety is also filled with an MeCN molecule. Mn2 is six coordinate and in a distorted octahedral geometry, the sixth site being filled by a dmf molecule. Gd1 is eight coordinate and in square antiprismatic geometry, the two terminally bonded O atoms (O9, O10) deriving from the pdm^{2−} and pdmH[−] ligands. The latter are H-bonded to the equivalent atoms on a neighbouring cluster (O(H)⋯O, ~3.4 Å), creating head-to-head dimeric units. Closest inter-cluster M⋯M distances occur neighbouring Gd ions at distances of ~6 Å.

The small nuclearity of the cluster, and the presence of the largely uncoordinated H₃TBC[4] moiety is ascribed to the presence of the 2,6-pyridinedimethanol molecules chelating Gd1, blocking/preventing further cluster growth. Indeed, **11** is the only complex in which the bisTBC[4] ligand is not fully deprotonated, and the only example in which a TBC[4] pocket has not chelated a metal ion. In this respect, one can see that the introduction of the 2,6-pyridinedimethanol co-ligand has not been complementary in the self-assembly process, stunting the growth of the cluster. That said, a new and interesting cluster has been formed – **11** being the first published example of a [Mn₂Gd] triangle containing both Mn^{III} and Mn^{II} ions. We also note that this unit appears in **8** and **10** and in the TBC[4]-supported [Mn₃Ln] butterflies.²⁴

Magnetic susceptibility and magnetisation measurements for **11** reveal the presence of both (weak) ferro- and antiferromagnetic exchange interactions (Fig. 15). A simultaneous fit of both data sets resulted in the best fit parameters $J_{\text{Mn(II)}-\text{Mn(III)}} = +0.42 \text{ cm}^{-1}$, $J_{\text{Mn(III)}-\text{Gd(III)}} = +0.22 \text{ cm}^{-1}$, $J_{\text{Mn(II)}-\text{Gd(III)}} = -0.26 \text{ cm}^{-1}$ and $D_{\text{Mn(III)}} = -4.1 \text{ cm}^{-1}$ (with the *g*-factors fixed at *g* = 2.00 for Mn^{II} and Gd^{III} and *g* = 1.98 for Mn^{III}). These parameters are similar to those found for the TBC[4]-supported [Mn^{III}Mn^{II}Gd^{III}] butterflies,²⁴ and complex **8**, above. The ground spin-state of **11** (using only the isotropic part of the spin-Hamiltonian) is *S* = 4, with multiple low-lying excited spin states. *Ab initio* calculations of model compounds based on **11** afford very similar values to the experimental fits, with $J_{\text{Mn(II)}-\text{Mn(III)}} = +0.50 \text{ cm}^{-1}$, $J_{\text{Mn(III)}-\text{Gd(III)}} = +0.10 \text{ cm}^{-1}$, $J_{\text{Mn(II)}-\text{Gd(III)}} = -0.16 \text{ cm}^{-1}$ and $D_{\text{Mn(III)}} = -3.3 \text{ cm}^{-1}$. Magneto-structural DFT calculations reveal that O3 (the central μ₃-bridging atom) has a spin density three times higher than any other bridging

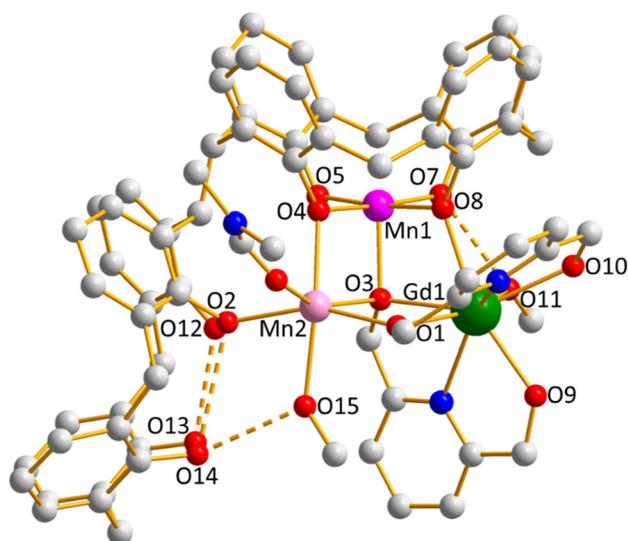


Fig. 14 Molecular structure of complex **11**. Colour code: Gd^{III} = dark green, Mn^{III} = magenta, Mn^{II} = pale pink, O = red, N = blue, Cl = light green, C = grey. H atoms, ^tBu groups, endo-cavity solvent, and solvent of crystallisation are omitted for clarity.



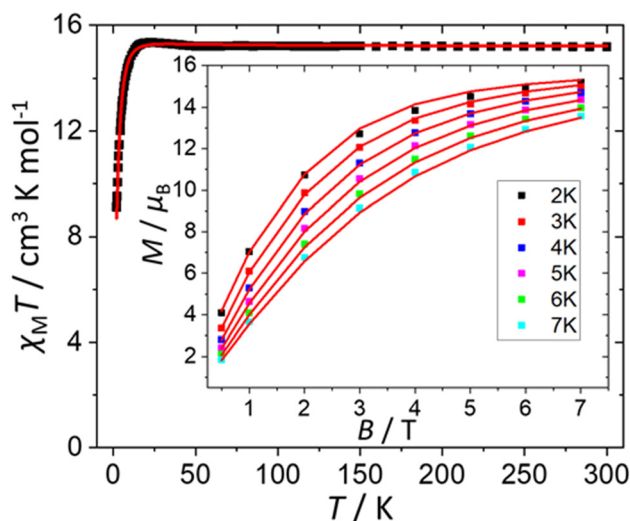


Fig. 15 Magnetic susceptibility and magnetisation (inset) data for **11**. The solid red lines represent a simultaneous fit of the experimental (squares) data. See text for details.

atoms, and therefore plays a dominant role in the magnetic exchange. For the Mn^{II/III}–Gd^{III} exchange pathway the Mn–O–Gd angle is the most dominant structural parameter, with a weak antiferromagnetic exchange observed at smaller angles, and a weak ferromagnetic interaction favoured at larger

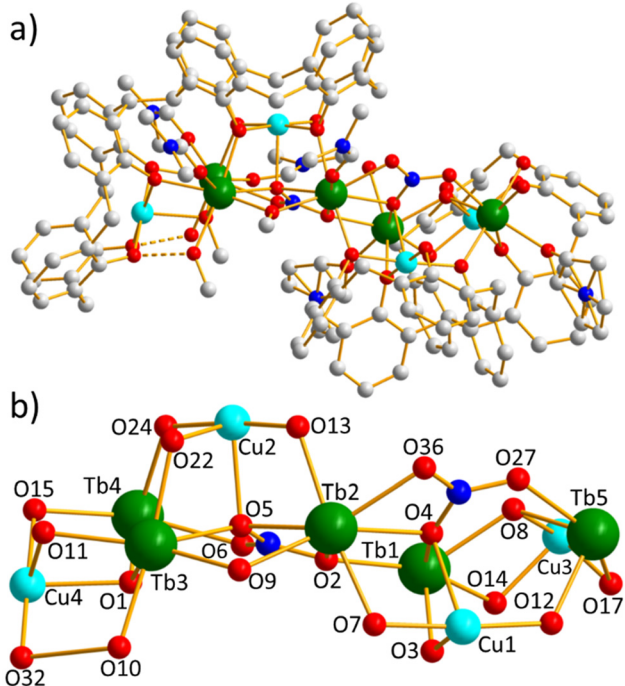


Fig. 16 (a) Molecular structure of complex **12**. (b) Metal–oxygen core of **12** highlighting the coordination of the nitrate anions. Colour code: Tb^{III} = dark green, Cu^{II} = pale blue, O = red, N = dark blue, Cl = light green, C = grey. H atoms, ^tBu groups, counter ions, endo-cavity solvent, and solvent of crystallisation are omitted for clarity.

angles. The weakly ferromagnetic Mn^{III}–Mn^{II} interaction is as expected from previous magneto-structural studies on this unit.^{5,6,24}

The remaining two heterometallic structures are [Cu^{II}Tb^{III}(bisTBC[4])₂(μ₃-OMe)(μ-OMe)(μ₃-OH)(μ₄-NO₃)(μ₅-NO₃)(MeOH)(dmf)₆(H₂O)₄](OH)₂·6dmf·H₂O (**12**·6dmf·H₂O) and [Fe^{III}Gd^{III}(bisTBC[4])₂(μ₄-O)₂(μ₃-O)₂(μ₃-NO₃)₂(dmf)₈(H₂O)₆](OH)·8dmf (**13**·8dmf) published in the same paper in 2017.¹³

The former is made *via* the reaction of Cu(NO₃)₂·3H₂O, Tb(NO₃)₃·6H₂O and H₈bisTBC[4] in a basic MeOH/dmf mixture. Crystals of **12**·6dmf·H₂O solve in the monoclinic space group *P*2₁/*n* upon slow evaporation of the mother liquor (Fig. 16).¹³ The asymmetric unit contains the whole formula. The metallic skeleton of **12** comprises of two [Cu^{II}Tb^{III}] butterflies (Cu1, Cu3, Tb1, Tb5; Cu2, Cu4, Tb3, Tb4), linked by a single, central Tb ion (Tb2). The two [Cu^{II}Tb^{III}] butterflies are rather similar. The first (Cu1, Cu3, Tb1, Tb5) consists of an asymmetric

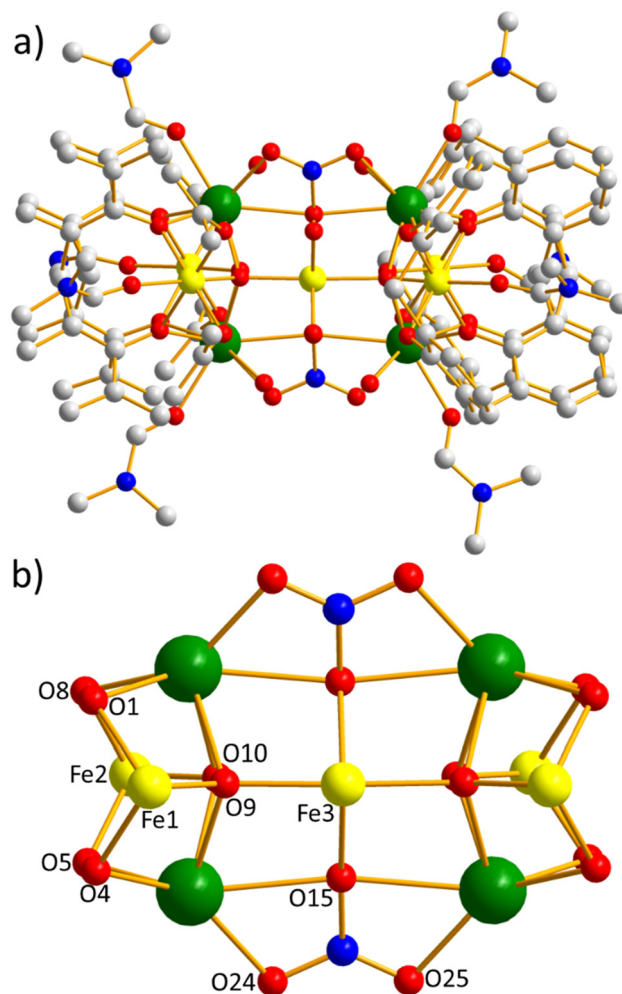


Fig. 17 (a) Molecular structure of complex **13**. (a) The metal–oxygen core of **13** highlighting the bridging on the nitrate ions. Colour code: Gd^{III} = dark green, Fe^{III} = yellow, O = red, N = dark blue, Cl = light green, C = grey. H atoms, ^tBu groups, counter ions and solvent of crystallisation are omitted for clarity.



[Cu^{II}Tb^{III}(μ₃-OH)(μ-OR)₄(O(NO₃))] unit, with the Tb^{III} ions in the body and the Cu^{II} ions in the wings. The μ-OH⁻ ion (O8) bridges between Tb1 and Tb5 and to Cu3 at the periphery of the cluster. The four edges of the butterfly are bridged by μ-O(Ph) atoms (O3, O12, O14, O17) originating from the same calixarene ligand. Tb1, Tb5 and Cu1 are further linked *via* a μ₄-NO₃⁻ ion: O4 bridging between Cu1 and Tb1 and further bridging to the central Tb2 ion, O27 is bonded terminally to Tb5, and O36 bonded terminally to Tb2. The second [Cu^{II}Tb^{III}(μ₃-OMe)(μ-OR)₄(O(NO₃))] butterfly differs from the first only in the replacement of the μ₃-OH⁻ ion with a μ₃-OMe⁻ ion (O1), which links Tb3, Tb4 and Cu4.

The bisTBC[4] ligands are fully deprotonated and both bridge in the same μ₅-fashion, with three terminally bonded O atoms and five μ-bridging O atoms. The former are H-bonded to the O atoms of H₂O/MeOH molecules coordinated to the Tb ions in the body positions of the butterflies. In turn, both are H-bonded to H₂O molecules of crystallisation, some of the latter also being H-bonded to the μ₅-NO₃⁻ ion. The Cu^{II} ions are housed in the pockets of the TBC[4] moieties and are five coordinate, in distorted square pyramidal geometries. They have a longer, sixth contact to a molecule of dmf that sits in each calixarene cavity. The direction perpendicular to the plane of the four O(Ph) atoms is the Jahn–Teller axis, as seen in the Mn-based complexes above. Four of the Tb^{III} ions (Tb1, Tb3, Tb4, Tb5) are seven coordinate and pentagonal bipyramidal, while Tb2 is eight coordinate and square antiprismatic.

The dmf and H₂O molecules of crystallisation are H-bonded to each other, and as both are situated in the space between molecules of **12**, this gives rise to head-to-head dimeric cluster units in the extended structure. The closest metal–metal inter-cluster distance is along the *b* axis of the

cell at ~13 Å. Note the structural similarity of complex **11** to complex **2**, **3**, **7** and **10**. Magnetic susceptibility and magnetisation data for **12** reveal the presence of weak antiferromagnetic exchange between the constituent metal ions.

The same reaction as above (for **12**) but using Fe(NO₃)₃·6H₂O, and Gd(NO₃)₃·6H₂O leads to the isolation of compound **13**, crystals of which solve in the triclinic space group *P* $\bar{1}$ (Fig. 17).¹³ The asymmetric unit contains half the formula. The metallic skeleton describes two [Fe^{III}Gd^{III}] butterflies encapsulating a single, central Fe^{III} ion (Fe3, disordered over two positions†). The butterflies are [Fe^{III}Gd^{III}O₂(OR)₄] with Gd1 and Gd2 (and *s.e.*) occupying the body positions and Fe1, Fe2 occupying the wing positions. Two μ_{3/4}-O²⁻ ions sit in the centre of the butterfly, connecting the body to the wings, further bridging to Fe3. Each edge of the butterfly is μ-bridged by an O atom deriving from the same calixarene ligand. Fe3 is further connected to the butterflies through two μ₃-NO₃⁻ ions (disordered over two positions), that cap the Gd...Gd (Gd1, Gd2) edge. Each bisTBC[4] ligand is μ₄-bridging, connected only to the metal ions in one butterfly. Thus, four of its O atoms are μ-bridging and four are terminally bound. The latter H-bond to the O atoms of the H₂O molecules completing the coordination spheres of Fe3 and the Gd ions. The H₂O molecules are also H-bonded to each other. The Fe^{III} ions are all six coordinate and in distorted octahedral geometries, the coordination sphere of the four Fe^{III} ions housed in the TBC[4] pockets being completed by a molecule of dmf that sits in each calixarene cavity. The Gd^{III} ions are eight coordinate and have distorted square antiprismatic geometries, a molecule of dmf completing the coordination sphere. Shortest inter-cluster contacts are between the ^tBu with C...H distances >4.5 Å. Closest inter cluster M...M distances are >14 Å.

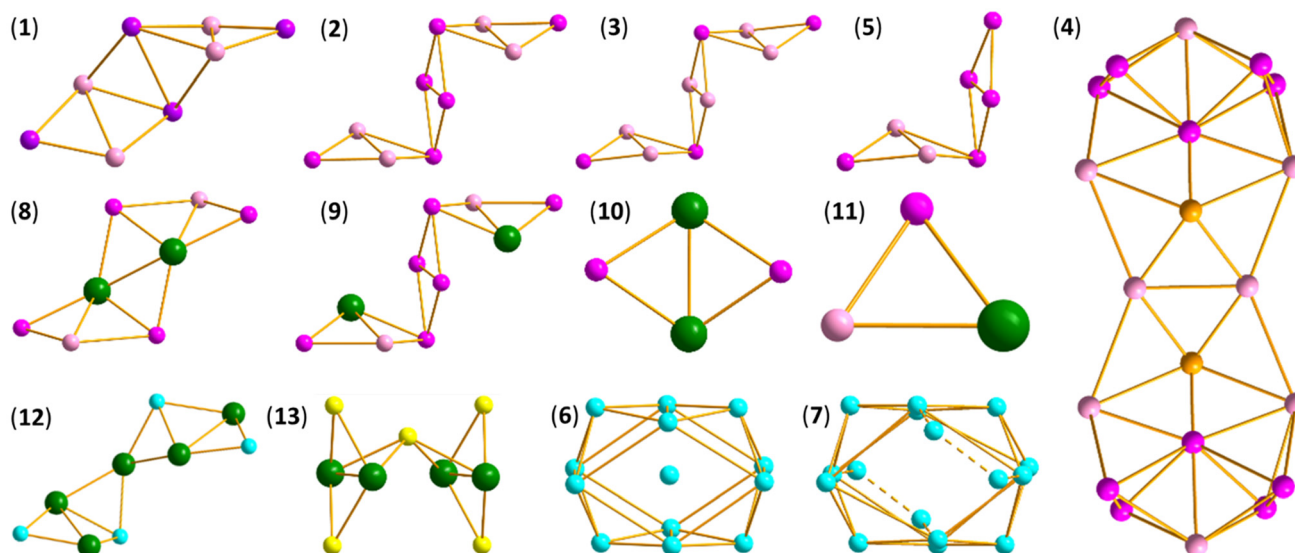


Fig. 18 The metallic skeletons of compounds **1**–**13**. The dominant structure directing effect of the bisTBC[4] ligand is reflected in both the presence of tetrametallic butterfly moieties and in the overall structural similarity of the thirteen compounds reported. Indeed, in some cases 'isostructural' species can be obtained with metal ions in different oxidation states, and even when replacing TM ions with LnM ions. Colour code: Mn^{III} = purple, Mn^{II} = pink, Ln^{III} = green, Fe^{III} = yellow, Cu^{II} = pale blue.



Magnetic susceptibility and magnetisation measurements on **13** reveal the presence of both ferro- and antiferromagnetic exchange interactions. The large nuclearity of **13**, aligned with the disorder present, prevents any rigorous quantitative analysis of the data. One might expect a large antiferromagnetic exchange *via* the Fe–O–Fe pathway, but the susceptibility data are rather flat from 300–50 K suggesting this is not the case – perhaps due to the disorder present. The Fe–Gd exchange in the butterflies would be expected to be very small. Magnetisation data to 7 T at $T = 2$ K saturates at $48\mu_{\text{B}}$, lower than the maximum expected for ferromagnetic exchange ($53\mu_{\text{B}}$), and equal to that expected if one $S = 5/2$ spin (Fe^{III}) is flipped.

Conclusions

The coordination chemistry of $\text{H}_8\text{bisTBC}[4]$ is clearly under explored, with only 13 structures known. These are limited to homometallic clusters of Mn and Cu, and heterometallic 3d–4f clusters of Mn–Gd, Fe–Gd and Cu–Tb. There are no homometallic clusters of V, Cr, Fe, Co or Ni, nor any homometallic 4f compounds. Thus, there is potential for a vast amount of new chemistry to be discovered. All thirteen structures have been made under ambient reaction conditions – there are no reports of any complex being made *via* solvothermal (or microwave, sonochemical) reaction methods. Solvothermal synthesis is often a good way of making high symmetry species, and with paramagnetic materials, this may offer a route to complexes displaying spin frustration²⁷ and/or an enhanced magnetocaloric effect.²⁸

The topology/disposition of the inverted, fully deprotonated bisTBC[4] ligand places eight phenolates in close proximity (*via* convergent lower-rims), favouring the formation of $[\text{M}_4]$ butterflies, with two metals housed in the TBC[4] pockets (the wings) and two encapsulated in the space between these pockets (the body). The metal ions are linked, centrally, by either $\text{O}^{2-}/\text{OH}^-$ ions generated *in situ*. The four edges of the butterfly are most commonly occupied by $\mu\text{-O(Ph)}$ atoms deriving from the calixarene, producing $[\text{M}_4(\text{O/OH})_x(\text{OR})_4]$ units. A structural comparison of the metallic skeletons is given in Fig. 18, where the prevalence of butterflies is easily recognised. The dominant structure directing effect of the bisTBC[4] ligand is also reflected in the overall structural similarity of the thirteen compounds reported. Indeed, in some cases ‘isostructural’ species can be obtained with metal ions in different oxidation states, and even when replacing TM ions with LnM ions. This is rather unusual in 3d–4f chemistry, given the different coordination numbers and coordination preferences of the two metal types.

In only one compound (**11**) was the bisTBC[4] ligand found not to be fully deprotonated. This was as the result of the addition of the co-ligand pdmH_2 , which when coordinated as its mono- or dianion blocked coordination sites on the metal ion, hindering further calixarene bonding and cluster growth. On only one occasion (**5**) is the bisTBC[4] ligand present in both *syn*- and *anti*-conformations. The presence of the latter is likely due to the incorporation of the hmp^- co-ligands, which occupy significant space preventing ligand inversion. Thus, the

use of co-ligands clearly affects the self-assembly process, and remains a useful tool to vary structure type. When viewing the various bonding modes of the bisTBC[4] in **1–13** as a whole, the O(Ph) atoms are either μ -bridging or terminally bonded. The latter are almost always H-bonded to terminal solvent molecules. The calixarene binding modes observed range from μ_4 - to μ_8 -bridging, and the binding rules established for TBC[4] also apply to bisTBC[4] such that bonding to TM^{III} is preferred over TM^{II} which in turn is preferred over LnM^{III} .

Magnetic studies reveal the prevalence of competing (weak) ferro- and antiferromagnetic exchange in the Mn-based compounds. We note that $\text{Mn}^{\text{III}}\text{-Mn}^{\text{II}}$ exchange is almost always found to be weakly ferromagnetic, in agreement with literature examples, perhaps highlighting a strategy for constructing molecules with very large spin ground states. In some cases magnetic data, in combination with theoretical studies, has allowed for the development of detailed magneto-structural correlations. The magnetic properties of the Cu^{II} -based complexes are dominated by strong antiferromagnetic interactions. In the case of $[\text{Cu}_{13}]$ (**6**) it would be interesting to investigate whether a larger paramagnetic metal ion, *e.g.* LnM, could be encapsulated at its centre. An interesting example would be Gd^{III} , since $\text{Gd}^{\text{III}}\text{-Cu}^{\text{II}}$ interactions are almost always found to be ferromagnetic.²⁹ We note that in all cases, the large cluster nuclearity and the presence of multiple exchange interactions (and the associated large Hilbert spaces) makes fitting of experimental magnetic data very difficult, if not impossible.

Author contributions

SJD and EKB wrote the manuscript.

Conflicts of interest

There are no conflicts to declare.

Data availability

This review does not contain any new data. Readers are referred to the original manuscripts for further information.

Acknowledgements

SJD and EKB thank the EPSRC (EP/I03255X/1 and EP/I031421/1) for funding.

References

- 1 For example, see: I. Thondorf, A. Shivanyuk and V. Böhmer, in *Chapter 2 in Calixarenes 2001*, ed. Z. Asfari, V. Böhmer, J. Harrowfield and J. Vicens, Kluwer Academic Publishers, Dordrecht, 2001, and references therein.



- 2 I. Thondorf, in *Chapter 15 in Calixarenes 2001*, ed. Z. Asfari, V. Böhmer, J. Harrowfield and J. Vicens, Kluwer Academic Publishers, Dordrecht, 2001, and references therein.
- 3 C. Aronica, G. Chastanet, E. Zueva, S. A. Borshch, J. M. Clemente-Juan and D. Luneau, *J. Am. Chem. Soc.*, 2008, **130**(7), 2365–2371.
- 4 For a recent review on TBC[n]-supported Ti clusters please see: X.-Y. Chen, Q.-Y. Liu, W.-D. Yu, J. Yan and C. Liu, *Chem. Commun.*, 2024, **60**, 11890, and references therein.
- 5 (a) G. Karotsis, S. J. Teat, W. Wernsdorfer, S. Piligkos, S. J. Dalgarno and E. K. Brechin, *Angew. Chem., Int. Ed.*, 2009, **48**, 8285–8288; (b) S. M. Taylor, G. Karotsis, R. D. McIntosh, S. Kennedy, S. J. Teat, C. M. Beavers, W. Wernsdorfer, S. Piligkos, S. J. Dalgarno and E. K. Brechin, *Chem. – Eur. J.*, 2011, **17**, 7521–7530.
- 6 (a) E. K. Brechin, J. Yoo, M. Nakano, J. C. Huffman, D. N. Hendrickson and G. Christou, *Chem. Commun.*, 1999, 783–784; (b) J. Yoo, E. K. Brechin, A. Yamaguchi, M. Nakano, J. C. Huffman, A. L. Maniero, L.-C. Brunel, K. Awaga, H. Ishimoto, G. Christou and D. N. Hendrickson, *Inorg. Chem.*, 2000, **39**, 3615–3623.
- 7 S. M. Taylor, G. Karotsis, R. D. McIntosh, S. Kennedy, S. J. Teat, C. M. Beavers, W. Wernsdorfer, S. Piligkos, S. J. Dalgarno and E. K. Brechin, *Chem. – Eur. J.*, 2011, **17**, 7521–7530.
- 8 (a) J. M. Harrowfield, M. I. Ogden, A. H. White and F. R. Wilner, *Aust. J. Chem.*, 1989, **42**, 949–958; (b) S. M. Taylor, S. Sanz, R. D. McIntosh, C. M. Beavers, S. J. Teat, E. K. Brechin and S. J. Dalgarno, *Chem. – Eur. J.*, 2012, **18**, 16014–16022.
- 9 S. Du, H. Ke, Y. Bi, H. Tan, Y. Yu, J. Tang and W. Liao, *Inorg. Chem. Commun.*, 2013, **29**, 85–88.
- 10 L. T. Carroll, P. A. Hill, C. Q. Ngo, K. P. Klatt and J. L. Fantini, *Tetrahedron*, 2013, **69**, 5002–5007.
- 11 R. McLellan, M. A. Palacios, C. M. Beavers, S. J. Teat, S. Piligkos, E. K. Brechin and S. J. Dalgarno, *Chem. – Eur. J.*, 2015, **7**, 2804–2812.
- 12 Conquest, version 2.24.3.0, accessed 08/09/2025.
- 13 R. McLellan, M. A. Palacios, C. M. Beavers, S. J. Teat, S. Piligkos, E. K. Brechin and S. J. Dalgarno, *Chem. – Eur. J.*, 2015, **21**, 2804–2812.
- 14 T. C. Stamatatos and G. Christou, *Philos. Trans. R. Soc., A*, 2008, **366**, 113–125.
- 15 K. R. Vignesh, S. K. Langley, K. S. Murray and G. Rajaraman, *Chem. – Eur. J.*, 2015, **21**, 2881–2892.
- 16 M. Coletta, R. McLellan, A. Waddington, S. Sanz, K. J. Gagnon, S. J. Teat, E. K. Brechin and S. J. Dalgarno, *Chem. Commun.*, 2016, **52**, 14246–14249.
- 17 L. R. B. Wilson, M. Coletta, R. Jose, G. Rajaraman, S. J. Dalgarno and E. K. Brechin, *Dalton Trans.*, 2021, **50**, 17566–17572.
- 18 (a) N. Berg, T. Rajeshkumar, S. M. Taylor, E. K. Brechin, G. Rajaraman and L. F. Jones, *Chem. – Eur. J.*, 2012, **18**, 5906–5918; (b) K. R. Vignesh, S. K. Langley, C. J. Gartshore, B. Moubaraki, K. S. Murray and G. Rajaraman, *Inorg. Chem.*, 2017, **56**, 1932–1949; (c) C. J. Milios, R. Inglis, A. Vinslava, R. Bagai, W. Wernsdorfer, S. Parsons, S. P. Perlepes, G. Christou and E. K. Brechin, *J. Am. Chem. Soc.*, 2007, **129**, 12505–12511; (d) C. J. Milios, M. Manoli, G. Rajaraman, A. Mishra, L. E. Budd, F. White, S. Parsons, W. Wernsdorfer, G. Christou and E. K. Brechin, *Inorg. Chem.*, 2006, **45**, 6782–6793.
- 19 See for example: (a) A. J. Tasiopoulos and S. P. Perlepes, *Dalton Trans.*, 2008, 5537–5555; (b) J. W. Sharples and D. Collison, *Coord. Chem. Rev.*, 2014, **260**, 1–20.
- 20 M. Coletta, S. Sanz, L. J. McCormick, S. J. Teat, E. K. Brechin and S. J. Dalgarno, *Dalton Trans.*, 2017, **46**, 16807–16811.
- 21 M. Coletta, S. Sanz, E. K. Brechin and S. J. Dalgarno, *Dalton Trans.*, 2020, **49**, 9882–9887.
- 22 G. Karotsis, S. Kennedy, S. J. Dalgarno and E. K. Brechin, *Chem. Commun.*, 2010, **46**, 3884–3886.
- 23 L. R. B. Wilson, M. Coletta, M. K. Singh, S. J. Teat, A. Brookfield, M. Shanmugam, E. J. L. McInnes, S. Piligkos, S. J. Dalgarno and E. K. Brechin, *Dalton Trans.*, 2023, **52**, 8956–8963.
- 24 M. A. Palacios, R. McLellan, C. M. Beavers, S. J. Teat, H. Weihe, S. Piligkos, S. J. Dalgarno and E. K. Brechin, *Chem. – Eur. J.*, 2015, **21**, 11212–11218.
- 25 M. Coletta, R. McLellan, S. Sanz, K. J. Gagnon, S. J. Teat, E. K. Brechin and S. J. Dalgarno, *Chem. – Eur. J.*, 2017, **23**, 14073–14079.
- 26 M. Coletta, S. Sanz, D. J. Cutler, S. J. Teat, K. J. Gagnon, M. K. Singh, E. K. Brechin and S. J. Dalgarno, *Dalton Trans.*, 2020, **49**, 14790–14797.
- 27 J. Schnack, *Dalton Trans.*, 2010, **39**, 4677–4686.
- 28 M. Evangelisti and E. K. Brechin, *Dalton Trans.*, 2010, **39**, 4672–4676.
- 29 J. Paulovic, F. Cimpoesu, M. Ferbinteanu and K. Hirao, *J. Am. Chem. Soc.*, 2004, **126**, 3321–3331.

